

Symmetry indicators in commensurate magnetic flux

Yuan Fang¹ and Jennifer Cano^{1,2}

¹*Department of Physics and Astronomy, Stony Brook University, Stony Brook, New York 11974, USA*

²*Center for Computational Quantum Physics, Flatiron Institute, New York, New York 10010, USA*
(Dated: June 19, 2023)

We derive a framework to apply topological quantum chemistry in systems subject to magnetic flux. We start by deriving the action of spatial symmetry operators in a uniform magnetic field, which extends Zak’s magnetic translation groups to all crystal symmetry groups. Ultimately, the magnetic symmetries form a projective representation of the crystal symmetry group. As a consequence, band representations acquire an extra gauge invariant phase compared to the non-magnetic theory. Thus, the theory of symmetry indicators is distinct from the non-magnetic case. We give examples of new symmetry indicators that appear at π flux. Finally, we apply our results to an obstructed atomic insulator with corner states in a magnetic field. The symmetry indicators reveal a topological-to-trivial phase transition at finite flux, which is confirmed by a Hofstadter butterfly calculation. The bulk phase transition provides a new probe of higher order topology in certain obstructed atomic insulators.

I. INTRODUCTION

Threading magnetic flux through a two-dimensional crystal changes the single particle band spectrum into a Hofstadter butterfly spectrum that exhibits a fractal structure with an infinitude of mini gaps [1]. The Hofstadter butterfly is the lattice counterpart of Landau levels in the continuum. While the Landau levels of a continuum model are often easier to compute than the Hofstadter butterfly of the corresponding lattice model, diagnosing band topology in the presence of magnetic flux requires the lattice because topological invariants are defined over the entire Brillouin zone. The topology of Hofstadter bands has been a subject of intense recent study [2–7].

In the absence of magnetic flux, the topology of a band structure can be classified by the theory of topological quantum chemistry (TQC) [8–15]. A practical diagnosis comes from studying the space group representations of bands at high symmetry momenta, which are known as symmetry indicators [16]. However, in its present form, TQC cannot be directly applied to systems in a magnetic field because it does not account for the Aharonov-Bohm phase.

In the present manuscript we derive a framework to generalize TQC and the classification of symmetry indicators to band structures in the presence of a rational magnetic flux per unit cell. The workflow is shown in Fig. 1. We find that the two key ingredients in the theory of TQC – the irreducible representations of bands at high symmetry points in momentum space and the induced representations of localized orbitals in real space – are modified from their non-magnetic counterparts due to the presence of magnetic flux. The essential reason for this modification is that the commutation relations between crystal symmetries change in the presence of magnetic flux due to the Aharonov-Bohm phase. As a result, the symmetry operators form non-trivial projective representations of the space group. The earliest example of this is Zak’s magnetic translation group [17, 18]. Our

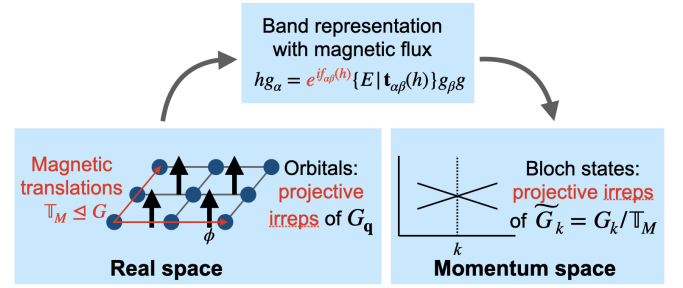


FIG. 1. Framework for TQC in the presence of magnetic flux. A representation of the site-symmetry group induces a band representation of the entire space group, which is subduced to a representation of the little co-group at each high-symmetry momentum, i.e., the symmetry indicator. The new element introduced by the magnetic field is that the symmetry operators form a projective representation of the space group. The red font indicates differences between TQC with and without magnetic flux.

theory builds on Zak’s theory by including crystalline symmetries.

Our theory of TQC in commensurate magnetic flux is distinct from “magnetic TQC” [15]. While magnetic TQC classifies topological band structures according to the representations of magnetic space groups, which describe the symmetry of magnetically ordered crystals, magnetic TQC does not yet accommodate magnetic flux through each unit cell, as it deals with zero flux configurations of orbitals.

The mathematical formalism utilized in this manuscript is also distinct from (magnetic) TQC. Specifically, (magnetic) TQC uses the usual linear (co-) representations of point groups, which were tabulated prior to those works. In contrast, our present study requires projective representations. The projective representations of point groups are not systematically tabulated. We derive an algorithm to construct magnetic symmetry operators using irreducible projective repre-

sentations of point groups. Our algorithm provides a framework that encompasses Zak's magnetic translation groups [17, 18], as well as the Benalcazar-Bernevig-Hughes model [19, 20]. We then use the magnetic symmetry operators to derive symmetry indicators for topological phases on lattices with a particular symmetry group and subject to commensurate flux. We give several explicit examples that have not appeared in previous literature.

Our manuscript proceeds as follows. In Sec. II, we derive the space group symmetry operators at rational flux in both real and momentum space. The results are at the crux of the theory of TQC in a magnetic field that we derive in Sec. IV. We then use the theory to compute symmetry indicators for magnetic layer groups, $p2$, $p4$, $p3$, $p6$, and $p4/m'$, at π flux per unit cell. The strong indicator in $p2$ recovers an earlier formula for the Chern number in Ref. 21, which is a stronger version of the formula in Ref. 22. In group $p4/m'$, our theory gives rise to a new strong \mathbb{Z}_2 indicator, which is simply the filling per unit cell mod 2. This \mathbb{Z}_2 non-trivial phase is protected by translation symmetry: the non-trivial phase does not permit exponentially localized and symmetric Wannier functions, but such Wannier functions exist when translation symmetries within the magnetic unit cell are broken. The Chern number indicators for $p3$, $p4$, and $p6$ do not appear in earlier work.

In Sec. V, we study a tight binding model introduced in Ref. 23 that realizes an obstructed atomic limit (OAL) on the square lattice at zero flux. The Hofstadter butterfly spectrum shows that the system undergoes a gap-closing phase transition at finite flux after which the corner states that were present in the OAL phase disappear. By applying our theory of TQC in a magnetic field to this model, we show that the gap closing corresponds to a phase transition from an OAL to a trivial phase that can be diagnosed by symmetry indicators.

II. MAGNETIC SYMMETRIES

In quantum mechanics the coupling of a magnetic field to a charged particle is described by replacing the momentum \mathbf{P} of the particle with the canonical momentum $\mathbf{p} = \mathbf{P} + \mathbf{A}$ in the Hamiltonian (without loss of generality, we have used natural units and assumed positive unit charge). To account for the Aharonov-Bohm phase, terms in the single-particle tight binding Hamiltonian are modified by the usual Peierls substitution:

$$c_{\mathbf{r}_2}^\dagger c_{\mathbf{r}_1} \mapsto e^{i \int_{\mathbf{r}_1}^{\mathbf{r}_2} \mathbf{A}(\mathbf{r}) \cdot d\mathbf{r}} c_{\mathbf{r}_2}^\dagger c_{\mathbf{r}_1}, \quad (1)$$

where the path of the integral is the straight line connecting \mathbf{r}_1 and \mathbf{r}_2 .

However, if the zero-field Hamiltonian is invariant under a crystal symmetry $\hat{g} : c_{\mathbf{r}} \mapsto c_{\hat{g}\mathbf{r}}$, the Hamiltonian modified by the Peierls substitution in Eq. (1) is not necessarily invariant under \hat{g} , even if the physical system

is unchanged by the symmetry. Consequently, the operator \hat{g} must be modified from its zero-field form by a gauge transformation that accounts for the Aharonov-Bohm phase. Specifically, the magnetic field requires \hat{g} be replaced by $g \equiv \tilde{G}_g \hat{g}$, where $\tilde{G}_g = e^{i \sum_{\mathbf{x}} \lambda_g(\mathbf{x}) c_{\mathbf{x}}^\dagger c_{\mathbf{x}}}$ is a gauge transformation that acts on the electron annihilation operators by [2]:

$$\tilde{G}_g c_{\mathbf{r}} \tilde{G}_g^{-1} = e^{-i \lambda_g(\mathbf{r})} c_{\mathbf{r}}, \quad (2)$$

$$\tilde{G}_g c_{\mathbf{r}}^\dagger \tilde{G}_g^{-1} = e^{i \lambda_g(\mathbf{r})} c_{\mathbf{r}}^\dagger, \quad (3)$$

where λ_g is a scalar function defined for each symmetry \hat{g} that we will derive momentarily. Acting on terms in the Hamiltonian in the form of Eq. (1), \tilde{G}_g has the effect of mapping $\mathbf{A}(\mathbf{r}) \mapsto \mathbf{A}(\mathbf{r}) + \nabla \lambda_g(\mathbf{r})$.

Similar gauge transformations were introduced by Zak for the magnetic translation operators in Refs. [17, 18]. More recently, the magnetic operators for rotations about the origin and for time-reversal symmetry were considered in Refs. [2, 21, 24]. Here, we develop a general theory for any symmetry group in the presence of a magnetic field, thereby extending previous works to include more general rotations and glide reflection symmetries. Doing so allows us to apply the theory of symmetry indicators to diagnose topological phases in the presence of a magnetic field.

We now derive the gauge transformation λ_g in Eq. (2): we require that if a single-particle Hamiltonian in zero field is invariant under a symmetry \hat{g} , then in the presence of a magnetic field that preserves \hat{g} , the Hamiltonian modified by the Peierls substitution in Eq. (1) is invariant under the combined symmetry operation $g \equiv \tilde{G}_g \hat{g}$, i.e., we require

$$g : e^{i \int_{\mathbf{r}_1}^{\mathbf{r}_2} \mathbf{A}(\mathbf{r}) \cdot d\mathbf{r}} c_{\mathbf{r}_2}^\dagger c_{\mathbf{r}_1} \mapsto e^{i \int_{g\mathbf{r}_1}^{g\mathbf{r}_2} \mathbf{A}(\mathbf{r}') \cdot d\mathbf{r}'} c_{g\mathbf{r}_2}^\dagger c_{g\mathbf{r}_1} \quad (4)$$

Acting on the left-hand-side by $g = \tilde{G}_g \hat{g}$, using the definition of \tilde{G}_g in Eqs. (2) and (3), and equating with the right-hand-side yields

$$e^{i \int_{\mathbf{r}_1}^{\mathbf{r}_2} \mathbf{A}(\mathbf{r}) \cdot d\mathbf{r} + i \int_{g\mathbf{r}_1}^{g\mathbf{r}_2} \nabla \lambda(\mathbf{r}') \cdot d\mathbf{r}'} = e^{i \int_{g\mathbf{r}_1}^{g\mathbf{r}_2} \mathbf{A}(\mathbf{r}') \cdot d\mathbf{r}'} \quad (5)$$

A few lines of algebra (detailed in Appendix A) show that Eq. (5) is satisfied when $\lambda_g(\mathbf{r})$ satisfies

$$\nabla \lambda_g(\mathbf{r}) = \mathbf{A}(\mathbf{r}) - R_g \mathbf{A}(g^{-1}\mathbf{r}), \quad (6)$$

where R_g is the point group part of g . Eq. (6) applies equally well to uniform or non-uniform magnetic fields. For simplicity, we restrict ourselves to the uniform field case for the remainder of this manuscript. Eq. (6) determines each λ_g up to a constant. We choose the constant such that for translation [2]

$$\lambda_{T(\mathbf{a})}(\mathbf{r}) = \int_{\mathbf{r}-\mathbf{a}}^{\mathbf{r}} \mathbf{A}(\mathbf{r}') \cdot d\mathbf{r}' + \mathbf{B} \cdot \mathbf{a} \times \mathbf{r} \quad (7)$$

and that a 2π rotation is implemented by the identity matrix. This choice of constants ensures that the commutation relations between translation and rotations about the origin are the same as at zero field as we show in the Appendix B. This choice of gauge is fixed throughout this paper; later when we refer to a gauge choice, we are referring to the gauge of the vector potential. So far, we have only considered lattice degrees of freedom; orbital and spin degrees of freedom can be included by an extra unitary transformation in the action of \hat{g} , which does not change λ_g . We will include these degrees of freedom in later sections.

Eq. (6), which serves as the definition of λ_g , is the first key result of this manuscript. Combining it with the spatial action of the symmetry yields the explicit form of the magnetic symmetry operator:

$$g = e^{i \sum_{\mathbf{x}'} \lambda_g(\mathbf{x}') c_{\mathbf{x}'}^\dagger c_{\mathbf{x}'}} \sum_{\mathbf{x}} c_{\hat{g}\mathbf{x}}^\dagger c_{\mathbf{x}} \quad (8)$$

$$= \sum_{\mathbf{x}} e^{i \lambda_g(\hat{g}\mathbf{x})} c_{\hat{g}\mathbf{x}}^\dagger c_{\mathbf{x}}, \quad (9)$$

where λ_g is determined by Eq. (6). The second equality holds when g acts on the single-particle Hilbert space.

We now explain why changing λ_g up to a constant does not change the representation of the magnetic symmetry operators defined in Eq. (9). These operators furnish projective representations of the space group. A projective representation ρ of a group satisfies the following multiplication rule

$$\rho(h_1)\rho(h_2) = \omega(h_1, h_2)\rho(h_1 h_2), \quad (10)$$

where h_1, h_2 are group elements and $\omega(h_1, h_2)$ is called the 2-cocycle. If $\omega(h_1, h_2) \equiv 1$, then ρ is an ordinary linear representation. In general, the magnetic symmetry operators in Eq. (9) will have non-trivial 2-cocycles, as we show in the next sections. The $U(1)$ gauge freedom in Eq. (6) corresponding to the gauge transformation $\lambda_g \mapsto \lambda_g + C_g$, $g \mapsto e^{iC_g}g$ leaves the representation in the same group cohomology class, i.e. the transformed projective representation is equivalent to the previous one. Essential properties of projective representations are presented in Appendix C.

In the next two subsections, we apply this formalism to two examples, first rederiving Zak's magnetic translation group and then reviewing the symmetries of the square lattice in a magnetic field.

A. Zak's magnetic translation group

In Refs. 17 and 18 Zak introduced the continuous magnetic translation symmetries. We reproduce Zak's result by taking the continuum limit of Eq. (9).

Consider a two-dimensional infinite plane without a lattice and denote operators that translate by $\Delta = \Delta_x \hat{x} + \Delta_y \hat{y}$ by $\hat{T}(\Delta) \equiv \hat{T}(\Delta_x, \Delta_y)$, where \hat{x} and \hat{y} denote the unit vectors.

We first work in the symmetric gauge: $\mathbf{A}(\mathbf{r}) = \frac{B}{2}(-r_y, r_x)$. Then from Eq. (6):

$$\lambda_{T(\Delta)}(\mathbf{r}) = \frac{B}{2}(\Delta_x r_y - \Delta_y r_x) \quad (11)$$

For continuous translations, we replace the sum $\sum_{\mathbf{x}} c_{\hat{T}(\Delta)\mathbf{x}}^\dagger c_{\mathbf{x}}$ in Eq. (8) with $e^{-ip_x \Delta_x - ip_y \Delta_y}$. Then the magnetic translation by vector Δ is

$$\begin{aligned} T(\Delta) &= e^{i(\frac{1}{2}B\Delta_x(r_y + \Delta_y) - \frac{1}{2}B\Delta_y(r_x + \Delta_x))} e^{-i(p_x \Delta_x + p_y \Delta_y)} \\ &= e^{-i((p_x - \frac{1}{2}Br_y)\Delta_x + (p_y + \frac{1}{2}Br_x)\Delta_y)}, \end{aligned} \quad (12)$$

where the Baker–Campbell–Hausdorff formula is considered. Therefore, the generators of the magnetic translations in \hat{x} and \hat{y} directions are

$$\begin{aligned} K_x &= p_x - \frac{1}{2}Br_y \\ K_y &= p_y + \frac{1}{2}Br_x, \end{aligned} \quad (13)$$

which is exactly Zak's definition from his 1964 paper [17].

In the remainder of the manuscript it will be easier to use the Landau gauge $\mathbf{A}(\mathbf{r}) = (-Br_y, 0)$. Repeating the calculation of λ_g in the Landau gauge yields

$$\lambda_{T(\Delta)}(\mathbf{r}) = -B\Delta_y r_x \quad (14)$$

One important property of the magnetic translation operators is the gauge-invariant noncommutativity:

$$T(\Delta_x \hat{x})T(\Delta_y \hat{y}) = T(\Delta_y \hat{y})T(\Delta_x \hat{x})e^{iB\Delta_x \Delta_y}, \quad (15)$$

which reproduces the Aharonov–Bohm phase. More generally, for two translations \mathbf{a}_1 and \mathbf{a}_2 , the gauge invariant multiplication equation is [17]

$$T(\mathbf{a}_1)T(\mathbf{a}_2) = T(\mathbf{a}_1 + \mathbf{a}_2)e^{\frac{i}{2}\mathbf{B} \cdot (\mathbf{a}_1 \times \mathbf{a}_2)} \quad (16)$$

The gauge invariant phase term $e^{\frac{i}{2}\mathbf{B} \cdot (\mathbf{a}_1 \times \mathbf{a}_2)}$ is the 2-cocycle of magnetic translations, which shows the magnetic translation operators form a non-trivial projective representation of the translation group.

B. Magnetic symmetries of the square lattice

As a second example, we consider discrete symmetries of the two-dimensional square lattice using the Landau gauge $\mathbf{A}(\mathbf{r}) = (-Br_y, 0)$. When $B = 0$, the square lattice is invariant under the layer group $p4/mmm$, which is generated by a four-fold rotation symmetry and the mirrors m_x and m_z . Without a magnetic field, the system is also invariant under time-reversal symmetry, \mathcal{T} .

When $B \neq 0$, only the symmetries that leave the magnetic field invariant (four-fold rotations and m_z) remain; the resulting layer group is $p4/m$. To determine how these symmetries act on the electron creation/annihilation operators, one must compute the

g	$T(\Delta_x \hat{\mathbf{x}})$	$T(\Delta_y \hat{\mathbf{y}})$	$C_2(\bar{x}, \bar{y})$	$C_4(\bar{x}, \bar{y})$	$I(\bar{x}, \bar{y})$	$Um_x(\bar{x})$	$Um_y(\bar{y})$
$\hat{g} = \{R_g \tau_g\}$	$\{0 (\Delta_x, 0)\}$	$\{0 (0, \Delta_y)\}$	$\{\hat{C}_2 (2\bar{x}, 2\bar{y})\}$	$\{\hat{C}_4 (\bar{x} + \bar{y}, \bar{y} - \bar{x})\}$	$\{\hat{I} (2\bar{x}, 2\bar{y})\}$	$U\{\hat{m}_x (2\bar{x}, 0)\}$	$U\{\hat{m}_y (0, 2\bar{y})\}$
$\lambda_g(x, y)$	0	$-B\Delta_y x$	$-2B\bar{y}(x - \bar{x})$	$-B(x - \bar{x})(y - \bar{y}) + B\bar{y}((y - \bar{y}) - (x - \bar{x}))$	$-2B\bar{y}(x - \bar{x})$	0	$-2B\bar{y}x$

TABLE I. The gauge transformation $\lambda_g(x, y)$ for symmetries of the square lattice in Landau gauge. For each symmetry g in the first row, the second row lists the symmetry in the notation $\{R_g | \tau_g\}$, where $\hat{g} : \mathbf{r} \mapsto R_g \mathbf{r} + \tau_g$. The third row provides λ_g from Eq. (6).

gauge transformation λ_g from Eq. (6). We summarize the results in Table I. Notice that λ_g depends on the rotation or inversion center; thus, it is necessary to introduce the notation

$$C_n(\bar{x}, \bar{y}) \equiv T(\bar{x}, \bar{y}) C_n T(-\bar{x}, -\bar{y}) \quad (17)$$

to denote an n -fold rotation about the point (\bar{x}, \bar{y}) ; we use $C_n \equiv C_n(\bar{x} = 0, \bar{y} = 0)$ to denote a rotation about the origin. We adopt analogous notation for inversions and reflections about different points and planes.

The symmetries m_x , $m_{(110)}$ and \mathcal{T} flip the magnetic field and thus are not symmetries at finite B . However, the product of these symmetries with a magnetic flux shifting operator can leave the system invariant at special values of flux, as we now describe.

A lattice Hamiltonian coupled to a magnetic field is periodic in B : the period corresponds to the minimal magnetic field such that every possible closed hopping path encloses an integer multiple of 2π flux. Let ϕ denote the magnetic flux per unit cell and $\Phi = 2\pi n$ its periodicity, where n is an integer. Following Ref. [2], we define the unitary matrix U that shifts $\phi \mapsto \phi + \Phi$ by

$$U = e^{i \sum_{\mathbf{x}'} \lambda_U(\mathbf{x}') c_{\mathbf{x}'}^\dagger c_{\mathbf{x}'}} \quad (18)$$

$$\lambda_U(\mathbf{r}) = \int_{\mathbf{r}_0}^{\mathbf{r}} \tilde{\mathbf{A}}(\mathbf{r}) \cdot d\mathbf{r}, \quad (19)$$

where \mathbf{r}_0 is a reference lattice point and $\tilde{\mathbf{A}}$ is the magnetic vector potential corresponding to Φ flux, i.e., $\nabla \times \tilde{\mathbf{A}} = \Phi$.

Notice that for any symmetry g that flips $\phi \mapsto -\phi$, the product Ug is a symmetry in the special case where $\phi = \Phi/2$. In the case of the square lattice, the products Um_x , Um_y and $U\mathcal{T}$ are recovered as symmetries of the system at the special value of $\phi = \Phi/2$. We list the gauge transformations for Um_x and Um_y at $\phi = \Phi/2$ in Table I.

In the special case of a square lattice and Landau gauge, $\lambda_U = -\Phi y x$, where $x = (\mathbf{r} - \mathbf{r}_0) \cdot \hat{\mathbf{x}}$. Since Φ is a multiple of 2π and x, y are integers, this phase is also a multiple of 2π . The flux translation matrix is given by $U = \mathbb{I}$, where \mathbb{I} is the identity matrix.

In summary, we have explicitly extended Zak's translation operators in a magnetic field to the discrete symmetries of the square lattice. In Appendix D we generalize the results to the symmetries of the triangular lattice.

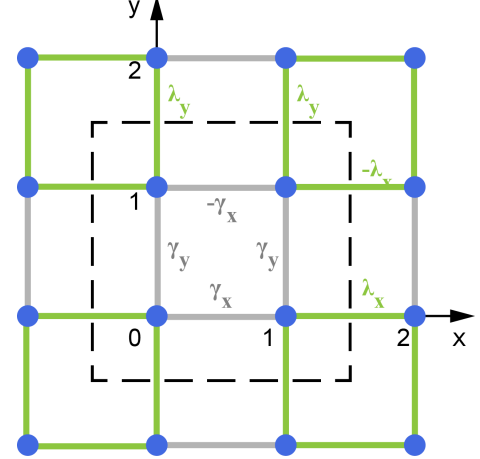


FIG. 2. Lattice and hopping terms of the BBH model. The black dashed square indicates the unit cell. Blue dots indicate atoms, each with one orbital. The origin is at the left-bottom atom in the unit cell indicated by 0. The hopping amplitudes $\gamma_{x/y}$ and $\lambda_{x/y}$ are real; the minus signs result from the magnetic flux $\phi = 4\pi$, i.e., applying Eq. (1) in Landau gauge.

C. BBH model

We apply the results of the previous section to derive the symmetry operators in the Benalcazar-Bernevig-Hughes (BBH) model [19, 20]. The model describes spinless electrons on a square lattice. The Hamiltonian consists of nearest-neighbor hopping terms, whose amplitudes $\lambda_{x/y}$ and $\gamma_{x/y}$ are depicted in Fig. 2. Since $\lambda_{x/y} \neq \gamma_{x/y}$, each unit cell contains four atoms. Further, each square plaquette has π flux, for a total flux $\phi = 4\pi$ per unit cell. The flux periodicity is $\Phi = 8\pi$, corresponding to 2π flux per square plaquette.

We now derive the symmetry operations in the presence of the magnetic field; these commutation relations were stated in Refs. 19 and 20, but here we derive them as an application of our formalism.

We start with the mirror symmetries: in zero field, the Hamiltonian is invariant under $m_x(\bar{x})$ and $m_y(\bar{y})$ where \bar{x}, \bar{y} are half-integers. (The Hamiltonian is not invariant under reflections about lines containing the origin because $\gamma_{x/y} \neq \lambda_{x/y}$.) These mirror reflections flip the sign of the magnetic field and thus generically are not symmetries of the Hamiltonian at finite flux. However, since $\phi = 4\pi = \Phi/2$, the combined operations $Um_x(\bar{x})$

and $Um_y(\bar{y})$ are symmetries. We showed in the previous section that in the Landau gauge, the flux shifting operator $U = \mathbb{I}$ for this model. Therefore, at $\phi = 4\pi$, $m_x(\bar{x})$ and $m_y(\bar{y})$ are in fact symmetries of the Hamiltonian. The effect of the magnetic field is to change their commutation relations: using Table I with $U = \mathbb{I}$ yields $m_x(\bar{x})m_y(\bar{y}) = m_y(\bar{y})m_x(\bar{x})e^{4iB\bar{x}\bar{y}}$. Since $B = \pi$ and \bar{x}, \bar{y} are half-integers

$$\{m_x(\bar{x}), m_y(\bar{y})\} = 0, \quad (20)$$

i.e., mirror symmetries in the BBH model anti-commute.

We now consider a four-fold rotation. When $\gamma_x = \gamma_y$, $\lambda_x = \lambda_y$, the BBH model has a four-fold rotation symmetry $C_4(\frac{1}{2}, \frac{1}{2})$, as well as other four-fold rotation axes related by translation. Since $\phi = \Phi/2$, the system also has an effective time-reversal symmetry, $U\mathcal{T}$; since we established $U = \mathbb{I}$ for this model, \mathcal{T} is a symmetry even at this finite field and acts by complex conjugation. In the absence of a magnetic field, time-reversal pairs eigenstates with $\pm i$ rotation eigenvalues. We now show that in the presence of a magnetic field, time-reversal pairs eigenstates of $C_4(\bar{x}, \bar{y})$ in a more complicated way.

Since our origin is chosen such that all lattice sites have integer coordinates, $x, y \in \mathbb{Z}$, the phase $e^{i\lambda c_4}$ in Table I takes values of $\pm e^{-i\pi/4}$, so that $e^{-2i\lambda c_4} = i$. Therefore, given an eigenstate $|\xi\rangle$ of $C_4(\bar{x}, \bar{y})$ with eigenvalue ξ , $\mathcal{T}|\xi\rangle$ is also an eigenstate of $C_4(\bar{x}, \bar{y})$:

$$\begin{aligned} C_4(\bar{x}, \bar{y})\mathcal{T}|\xi\rangle &= e^{i\lambda c_4}\hat{C}_4(\bar{x}, \bar{y})\mathcal{T}|\xi\rangle \\ &= \mathcal{T}e^{-i\lambda c_4}\hat{C}_4(\bar{x}, \bar{y})|\xi\rangle \\ &= \mathcal{T}e^{-2i\lambda c_4}C_4(\bar{x}, \bar{y})|\xi\rangle \\ &= \mathcal{T}i\xi|\xi\rangle = -i\xi^*\mathcal{T}|\xi\rangle. \end{aligned} \quad (21)$$

Thus, \mathcal{T} pairs $C_4(\bar{x}, \bar{y})$ eigenstates with eigenvalues ξ and $-i\xi^*$. This is an example of symmetry operators acting in unusual ways at finite field.

III. MOMENTUM SPACE REPRESENTATIONS

We now define how the magnetic symmetry operators act in momentum space. This requires first defining how the symmetries act on Bloch wave functions and then labelling the Bloch wave functions by irreducible representations (irreps) of the symmetry group at each momentum point. However, in the presence of magnetic flux, we cannot immediately define the Bloch wave functions because Bloch's theorem does not apply when the translation operators do not commute.

To apply Bloch's theorem, we define an enlarged “magnetic unit cell,” chosen to contain an integer multiple of 2π flux. The translation vectors that span the magnetic unit cell are referred to as magnetic translation vectors. From Eq. (15), the magnetic translation operators commute and thus can be simultaneously diagonalized, forming an abelian subgroup \mathbb{T}_M of the full translation group

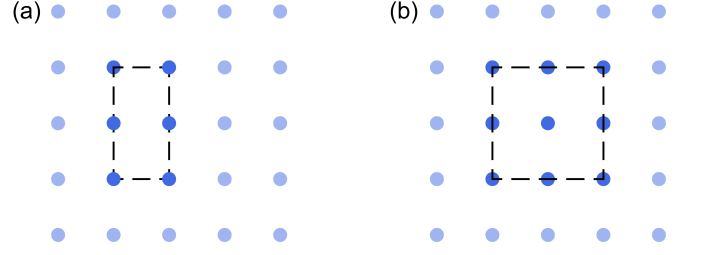


FIG. 3. Examples of (a) a q -by-1 unit cell and (b) a q -by- q unit cell, taking $q = 2$.

\mathbb{T} . Consequently, Bloch's theorem applies to the magnetic unit cell and eigenstates of the Hamiltonian can be labelled by wave vectors in the magnetic Brillouin zone.

In Sec. III A, we define the Fourier transformed electron creation and annihilation operators in the magnetic unit cell. The operators necessarily have a “sublattice” index because the magnetic unit cell contains more than one non-magnetic unit cell.

In Sec. III B, we address how to label the Bloch wave functions by irreps of the little co-group at each momentum. Here we encounter another subtle point: since the little co-group is defined as a quotient group obtained from the space group mod magnetic translations, the little co-group only has a group structure if the magnetic translation group is a normal subgroup of the space group. Thus, not all magnetic unit cells are equal: to label Bloch wave functions by irreps of the little co-group, we must choose a magnetic unit cell such that \mathbb{T}_M is a normal subgroup. After addressing this issue, we explain how to find the irreducible projective representations of the little co-group.

A. Symmetries in the magnetic Brillouin zone

We first consider the minimal magnetic unit cell in Landau gauge, which is a q -by-1 unit cell (see Fig. 3(a)). For this choice of unit cell, the magnetic translation group \mathbb{T}_M is generated by $T(\hat{\mathbf{x}})$ and $T(q\hat{\mathbf{y}})$.

Now consider the layer group $p2$, generated by C_2 and lattice translations, for which \mathbb{T}_M is a normal subgroup. C_2 acts identically to the non-magnetic case, mapping a Bloch wave function at \mathbf{k} to one at $-\mathbf{k}$. However, $T(\hat{\mathbf{y}})$ acts in an unusual way, by mapping k_x to $k_x + \phi$. This can be understood as follows: let $|\mathbf{k}\rangle$ be an eigenstate of $T(\hat{\mathbf{x}})$ such that $T(\hat{\mathbf{x}})|\mathbf{k}\rangle = e^{ik_x}|\mathbf{k}\rangle$. Then $T(\hat{\mathbf{y}})|\mathbf{k}\rangle$ is also an eigenstate of $T(\hat{\mathbf{x}})$, with eigenvalue $k_x + \phi$, i.e.,

$$T(\hat{\mathbf{x}})[T(\hat{\mathbf{y}})|\mathbf{k}\rangle] = e^{i(k_x + \phi)}T(\hat{\mathbf{y}})|\mathbf{k}\rangle \quad (22)$$

Thus, $T(\hat{\mathbf{y}})$ shifts the eigenvalue of $T(\hat{\mathbf{x}})$ by $e^{i\phi}$. Nonetheless, both C_2 and $T(\hat{\mathbf{y}})$ have the usual property that a Bloch state at \mathbf{k} is mapped to another Bloch state at \mathbf{k}' .

This is not the case for the layer group $p4$, with respect to which \mathbb{T}_M is not a normal subgroup. As we will show below, the symmetry operator C_4 mixes a Bloch

state at \mathbf{k} into a linear combination of Bloch states at other momenta, forming a q^2 -dimensional representation. Thus, we are motivated to consider a q -by- q unit cell (see Fig. 3(b)), where, although the magnetic unit cell is larger, the symmetry matrices are the same size as in the q -by-1 case. In Appendix E, we show that the representations obtained from these two choices of magnetic unit cell are the same up to a unitary transformation. However, the q -by- q unit cell is a more suitable to apply topological quantum chemistry because the corresponding magnetic translation group is a normal Abelian subgroup of the layer group $p4$. We now consider the q -by-1 and q -by- q unit cells in detail for the group $p4$ to illustrate these points.

1. q -by-1 unit cell for $p4$

We first consider the q -by-1 unit cell shown in Fig. 3(a). The coordinates of lattice sites are labeled by $(x, y) = (R_x, qR_y + j)$ where $R_x, R_y \in \mathbb{Z}$, $j = 0, \dots, q-1$. The Fourier transformed electron creation and annihilation operators are defined by

$$c_{\mathbf{R},j,\alpha}^\dagger = \frac{q}{(2\pi)^2} \int d\mathbf{k} e^{i(k_x R_x + k_y q R_y)} c_{\mathbf{k},j,\alpha}^\dagger \quad (23)$$

$$c_{\mathbf{R},j,\alpha} = \frac{q}{(2\pi)^2} \int d\mathbf{k} e^{-i(k_x R_x + k_y q R_y)} c_{\mathbf{k},j,\alpha}, \quad (24)$$

where α labels orbital degrees of freedom on each site. For now, we ignore the α degree of freedom, but will add it later when necessary. The magnetic Brillouin zone is a torus with $k_x \in [0, 2\pi)$, $k_y \in [0, 2\pi/q)$.

Using the Fourier transforms in Eqs. (23) and (24), we find the action of the symmetry operators in momentum space. A translation by one (non-magnetic) lattice vector in the \hat{y} direction is implemented by

$$T(\hat{y}) = \frac{q}{(2\pi)^2} \sum_j \int d\mathbf{k} e^{ik_y} c_{\mathbf{k}+(\phi,0),j}^\dagger c_{\mathbf{k},j-1} \quad (25)$$

Unlike the non-magnetic case, $T(\hat{y})$ does not leave each \mathbf{k} point invariant: it maps (k_x, k_y) to $(k_x + \phi, k_y)$. Translations by the magnetic lattice vectors do leave \mathbf{k} invariant.

We now consider the four-fold rotation operator. Using the function λ_{C_4} in Table I,

$$C_4 = \frac{q}{(2\pi)^2} \int d\mathbf{k} \sum_{j,j'} \sum_{n=0}^{q-1} \frac{1}{q} e^{i(\phi j j' - (k_y + 2\pi n/q)j - k_x j')} c_{(k_x, k_y),j}^\dagger c_{(k_y + 2\pi n/q, -k_x \bmod 2\pi/q),j'} \quad (26)$$

Thus, the situation for C_4 is much worse than for $T(\hat{y})$: C_4 does not rotate one \mathbf{k} point to another, but instead mixes a state at (k_x, k_y) into a linear combination of states at the different points $(k_y + 2\pi n/q, -k_x)$ $n = 0, 1, \dots, q-1$.

2. q -by- q unit cell for $p4$

We now consider the q -by- q unit cell shown in Fig. 3(b). The coordinates of lattice sites are labeled by $(x, y) = (qR_x + j_x, qR_y + j_y)$ where $R_x, R_y \in \mathbb{Z}$ label a magnetic unit cell and $j_x, j_y = 0, \dots, q-1$ label the coordinates of atoms within. The Fourier transformed electron creation and annihilation operators are defined by

$$c_{\mathbf{R},\mathbf{j},\alpha}^\dagger = \left(\frac{q}{2\pi}\right)^2 \int d\mathbf{k} e^{i(k_x q R_x + k_y q R_y)} c_{\mathbf{k},\mathbf{j},\alpha}^\dagger \quad (27)$$

$$c_{\mathbf{R},\mathbf{j},\alpha} = \left(\frac{q}{2\pi}\right)^2 \int d\mathbf{k} e^{-i(k_x q R_x + k_y q R_y)} c_{\mathbf{k},\mathbf{j},\alpha} \quad (28)$$

Again we omit the orbital degrees of freedom α in this section. The magnetic Brillouin zone is a torus with $k_x, k_y \in [0, 2\pi/q)$.

Using the Fourier transforms in Eqs. (27) and (28) and plugging λ_g from Table I into Eq. (9), the magnetic $T(\hat{y})$ and C_4 symmetries are [2]

$$T(\hat{y}) = \left(\frac{q}{2\pi}\right)^2 \int d\mathbf{k} e^{ik_y} \sum_{j_x, j_y} e^{-i\phi j_x} c_{\mathbf{k},j_x,j_y}^\dagger c_{\mathbf{k},j_x,j_y-1} \quad (29)$$

and

$$C_4 = \left(\frac{q}{2\pi}\right)^2 \int d\mathbf{k} \sum_{j_x, j_y} e^{-i\phi j_x j_y} e^{-i(C_4 \mathbf{k} \cdot \mathbf{j} - \mathbf{k} \cdot \mathbf{j}')} c_{(-k_y, k_x),j_x,j_y}^\dagger c_{(k_x, k_y),j'_x,j'_y} \quad (30)$$

where $\mathbf{j}' = (j'_x, j'_y)$ is a function of j_x, j_y that satisfies $j'_x = j_y \bmod q$ and $j'_y = -j_x \bmod q$. In Eqs. (29) and (30), the action of the symmetry operator on \mathbf{k} is identical to its action in the absence of a magnetic field, i.e., translation leaves \mathbf{k} invariant and a rotation in space rotates \mathbf{k} . This is an improvement over the q -by-1 magnetic unit cell (Eqs. (25) and (26)), for which a rotation mixed a Bloch state into a linear combination of several Bloch states.

B. Irreps at high symmetry points

We now address how to determine irreps of the symmetry group at each momentum. A Bloch wave function at a particular momentum \mathbf{k} transforms as a representation of the little group at \mathbf{k} , denoted $G_{\mathbf{k}}$, which consists of all the space group operations that leave \mathbf{k} invariant up to a reciprocal lattice vector:

$$G_{\mathbf{k}} = \{g \in G | g\mathbf{k} \equiv \mathbf{k}\}, \quad (31)$$

where \equiv is defined by equality up to a reciprocal lattice vector. Since the lattice translations are always represented by Bloch phases in the representations, it is useful to label the wave functions by irreps of the little co-group, defined as

$$\tilde{G}_{\mathbf{k}} = G_{\mathbf{k}} / \mathbb{T}_M \quad (32)$$

As mentioned above, for the little co-group to satisfy the definition of a group, \mathbb{T}_M must be a normal subgroup of $G_{\mathbf{k}}$, i.e., for all $g \in G_{\mathbf{k}}$, $t \in \mathbb{T}_M$, $g^{-1}tg \in \mathbb{T}_M$. One can check that for the q -by-1 unit cell, the magnetic translation group is a normal subgroup of the layer group $p2$, but it is not normal for the layer groups containing three- or four-fold rotations (because, for example, $C_4^{-1}T(\hat{\mathbf{x}})C_4 = T(\hat{\mathbf{y}})^{-1}$, which is not in the magnetic translation group for the q -by-1 unit cell.) Thus, we use the q -by- q unit cell for layer groups with three- or four-fold rotations.

Thus, under magnetic flux, the little co-groups and their irreps differ from their zero-flux analogues in two important ways: first, in the presence of magnetic flux, the little co-groups include sublattice translation symmetries; and second, the irreps of little co-groups in the presence of magnetic flux are projective representations corresponding to the 2-cocycle defined by the flux.

We now study some examples: in Tables II, III and IV we summarize the projective irreps at high symmetry points for the layer groups $p2$, $p4$, $p4/m'$ at flux $\phi = \pi$. For later convenience we have assumed there is spin-orbit coupling, i.e., $C_n^n = -1$. Notice that the character tables are not square, which is a general feature of projective representations. The projective irreps corresponding to a particular 2-cocycle can be considered as a subset of non-projective representations of a larger group; the character table of that larger group will be square.

To ensure that we have found all the projective irreps, we use the theorem by Schur [25] stating that for irreducible projective representations with a particular 2-cocycle,

$$\sum_{\rho} (\dim(\rho))^2 = |\tilde{G}_{\mathbf{k}}|, \quad (33)$$

where the sum runs over all projective irreps ρ of $\tilde{G}_{\mathbf{k}}$ with the specified 2-cocycle and $\tilde{G}_{\mathbf{k}}$ is the little co-group defined above. (Notice this formula does not apply to anti-unitary groups.)

The calculation of the irreps of little co-groups are shown in Appendix F with the (anti)-commutation relations for the magnetic symmetries shown in Appendix B. In the remainder of this section, we sketch the calculation for the simplest non-trivial case, layer group $p2$ at π flux.

For the 2-by-1 unit cell, the group of magnetic lattice translations is $\mathbb{T}_M = \{T(n_1\hat{\mathbf{x}} + 2n_2\hat{\mathbf{y}}) | n_1, n_2 \in \mathbb{Z}\}$ and the Brillouin zone is $[-\pi, \pi) \times [-\pi/2, \pi/2)$. We now determine the high-symmetry points. Since C_2 symmetry maps (k_x, k_y) to $(-k_x, -k_y)$, there are four momenta that are symmetric under C_2 up to a magnetic reciprocal lattice vector: $(0, 0)$, $(0, \pi/2)$, $(\pi, 0)$, $(\pi, \pi/2)$. Since $T(\hat{\mathbf{y}})$ maps (k_x, k_y) to $(k_x + \pi, k_y)$ (Eq. (22)), $T(\hat{\mathbf{y}})C_2$ maps (k_x, k_y) to $(-k_x + \pi, -k_y)$. Therefore, there are four $T(\hat{\mathbf{y}})C_2$ symmetric momenta, $(\pm\pi/2, 0)$ and $(\pm\pi/2, \pi/2)$.

We derive in Appendix F that the C_2 eigenvalues at $(\pi, 0)$ are the same as $(0, 0)$, while the C_2 eigenvalues

	$X(\pi/2, 0)$		$Y(0, \pi/2)$		$\Gamma(0, 0)$		$M(\pi/2, \pi/2)$	
Irrep	$X_1^{(p2)}$	$X_2^{(p2)}$	$Y_1^{(p2)}$	$Y_2^{(p2)}$	$\Gamma_1^{(p2)}$	$\Gamma_2^{(p2)}$	$M_1^{(p2)}$	$M_2^{(p2)}$
C_2			$+i$	$-i$	$+i$	$-i$		
$T(\hat{\mathbf{y}})C_2$	$+i$	$-i$					$+i$	$-i$

TABLE II. High symmetry momenta (first row) and the irreps (second row) of their little co-group for the group $p2$. The third and fourth rows list the eigenvalue of the indicated symmetry; the row is blank if the symmetry is not in the little co-group.

	$X(\pi/2, 0)$		$Y(0, \pi/2)$	
Irrep	X_1	X_2	Y_1	Y_2
C_2	$i\sigma_z$	$-i\sigma_z$	$i\sigma_z$	$-i\sigma_z$
$T(\hat{\mathbf{x}})$	σ_x	σ_x	σ_z	σ_z
$T(\hat{\mathbf{y}})$	σ_z	σ_z	σ_y	σ_y
$T(\hat{\mathbf{x}})T(\hat{\mathbf{y}})$	$-i\sigma_y$	$-i\sigma_y$	$-i\sigma_x$	$-i\sigma_x$

	$\Gamma(0, 0)$			
Irrep	Γ_1	Γ_2	Γ_3	Γ_4
$C_4T(\hat{\mathbf{x}})$	$\begin{pmatrix} 1 \\ i \end{pmatrix}$	$\begin{pmatrix} i \\ -1 \end{pmatrix}$	$\begin{pmatrix} -1 \\ -i \end{pmatrix}$	$\begin{pmatrix} -i \\ 1 \end{pmatrix}$
$T(\hat{\mathbf{x}})T(\hat{\mathbf{y}})$	$i\sigma_z$	$i\sigma_z$	$i\sigma_z$	$i\sigma_z$

	$M(\pi/2, \pi/2)$			
Irrep	M_1	M_2	M_3	M_4
C_4	$\begin{pmatrix} \epsilon \\ \epsilon^* \end{pmatrix}$	$\begin{pmatrix} -\epsilon^* \\ \epsilon \end{pmatrix}$	$\begin{pmatrix} -\epsilon \\ -\epsilon^* \end{pmatrix}$	$\begin{pmatrix} \epsilon^* \\ -\epsilon \end{pmatrix}$
$T(\hat{\mathbf{x}})T(\hat{\mathbf{y}})$	$i\sigma_z$	$i\sigma_z$	$i\sigma_z$	$i\sigma_z$

TABLE III. High symmetry momenta (first row) and the irreps (second row) of their little co-group for the group $p4$. Subsequent rows list the eigenvalue of the indicated symmetry with $\epsilon = e^{i\pi/4}$; the row is blank if the symmetry is not in the little co-group.

at $(0, \pi/2)$ are opposite of $(\pi, \pi/2)$. The same relations hold for the $T(\hat{\mathbf{y}})C_2$ symmetric points. In conclusion, there are two independent C_2 symmetric points, $\Gamma = (0, 0)$ and $Y = (0, \pi/2)$, and we find that each has two one-dimensional irreps labeled by C_2 eigenvalue $+i$, $-i$. There are also two independent $T(\hat{\mathbf{y}})C_2$ symmetric points, $X = (\pi/2, 0)$ and $M = (\pi/2, \pi/2)$, and each has two one-dimensional irreps labeled by $T(\hat{\mathbf{y}})C_2$ eigenvalue $+i$, $-i$. Since each little co-group contains the identity element and either C_2 or $T(\hat{\mathbf{y}})C_2$, $|\tilde{G}_{\mathbf{k}}| = 2$ for these points. Thus, Eq. (33) is satisfied, which means we have found all the projective irreps.

	$X(\pi/2, 0)$	$Y(0, \pi/2)$	$\Gamma(0, 0)$		$M(\pi/2, \pi/2)$		
Irrep	X_1X_2	Y_1Y_2	$\Gamma_1\Gamma_4$	$\Gamma_2\Gamma_3$	M_1M_1	M_3M_3	M_2M_4

TABLE IV. High symmetry momenta (first row) and the irreps (second row) of their little co-group for the group $p4/m'$. The notation $\Pi_i\Pi_j$ indicates that Π_i and Π_j are paired by \mathcal{TI} symmetry, where Π_i is an irrep of the corresponding little co-group with respect to layer group $p4$, shown in Table III.

IV. TOPOLOGICAL QUANTUM CHEMISTRY IN A MAGNETIC FIELD

Finally we turn to the theory of TQC. TQC classifies topological crystalline insulators (TCIs) by enumerating all trivial phases in each space group, where a trivial phase is defined as one where exponentially localized Wannier functions exist and transform locally under all symmetries. A group of bands can be identified as a TCI if it is not in the space of trivial phases.

Together, the Wannier functions corresponding to a single band (or group of bands) transform as a representation of the full space group, called a band representation [8, 11, 26–30]. TQC labels each band representation by how its Bloch wave functions transform under symmetry at high symmetry momenta, i.e., by a set of irreps of the little co-group at each high symmetry momentum; this label is known as a symmetry indicator [16]. Symmetry indicators provide a practical way to identify many TCIs: specifically, a group of bands whose irreps at high symmetry momenta are not consistent with any of the trivial phases must be topological.

In Sec. IV A we describe how to construct a basis of symmetric magnetic Wannier functions. We use this basis in Sec. IV B to derive how the space group symmetries act on the Wannier functions; the symmetry matrices comprise the band representation. Fourier transforming the band representation yields its symmetry indicator.

A. Magnetic Wannier functions

We now describe how to construct a basis of symmetric Wannier functions for a magnetic unit cell. Given a site \mathbf{q} , which will serve as a Wannier center, the site-symmetry group $G_{\mathbf{q}}$ is defined as the set of symmetries that leave \mathbf{q} invariant, i.e., $G_{\mathbf{q}} = \{g \in G | g\mathbf{q} = \mathbf{q}\}$. The site-symmetry group defines a coset decomposition of the space group,

$$G = \bigcup_{\alpha} g_{\alpha} G_{\mathbf{q}} \ltimes \mathbb{T}_M, \quad (34)$$

where G is the space group, \mathbb{T}_M is the magnetic lattice translation group, and $\alpha = 1, \dots, n$, where $n = |G/\mathbb{T}_M|/|G_{\mathbf{q}}|$ is the multiplicity of the Wyckoff position containing \mathbf{q} . The symmetries g_{α} are coset representatives. The choice of coset representatives is not unique; a different choice will yield a band representation related to the original by a unitary transformation, while the symmetry indicator is unchanged.

The coset representatives define positions $\mathbf{q}_{\alpha} = g_{\alpha}\mathbf{q}$ that form the orbit of \mathbf{q} within the magnetic unit cell. Together, these points are part of the same Wyckoff position, whose multiplicity n is equal to the number of points in the orbit of \mathbf{q} in the magnetic unit cell. Unlike the case of zero magnetic field, the set of coset representatives g_{α} includes pure translations within the magnetic unit cell.

Fig. 4 shows the Wyckoff positions for the groups $p2$, and $p4$, $p4/m'$.

Suppose there are $n_{\mathbf{q}}$ orbitals centered at \mathbf{q} . These orbitals are described by $n_{\mathbf{q}}$ Wannier functions $|W_{i1}\rangle$, where $i = 1 \dots n_{\mathbf{q}}$. The Wannier functions transform under symmetries $g \in G_{\mathbf{q}}$ as a projective representation ρ of $G_{\mathbf{q}}$,

$$g|W_{i1}\rangle = \sum_{j=1}^{n_{\mathbf{q}}} [\rho(g)]_{ji} |W_{j1}\rangle. \quad (35)$$

Applying the representatives g_{α} in the coset decomposition of the space group G in Eq. (34) to $|W_{i1}\rangle$ gives another Wannier function

$$|W_{i\alpha}\rangle = g_{\alpha}|W_{i1}\rangle, \quad (36)$$

localized at \mathbf{q}_{α} . All these Wannier functions $|W_{i\alpha}\rangle$, where $i = 1 \dots n_{\mathbf{q}}$ and $\alpha = 1 \dots n$, form an induced representation of G , as we now explain.

B. Induced representation

In this section, we derive how the space group symmetries act on the Wannier functions. This provides an explicit construction of a band representation with Wannier functions as a basis. Fourier transforming the band representation gives the irreps of the little co-group at each high-symmetry point, i.e., the symmetry indicator.

Consider a group element $hg_{\alpha} \in G$. The coset decomposition in Eq. (34) implies that hg_{α} can be written in the form

$$hg_{\alpha} = e^{if_{\alpha\beta}(h)} \{E|\mathbf{t}_{\alpha\beta}(h)\} g_{\beta} g \quad (37)$$

where $\mathbf{t}_{\alpha\beta}(h) = h\mathbf{q}_{\alpha} - \mathbf{q}_{\beta}$ and $\{E|\mathbf{t}_{\alpha\beta}\} \in \mathbb{T}_M$, $g \in G_{\mathbf{q}}$, and the coset representative g_{β} are uniquely determined by the coset decomposition. The remaining phase factor $f_{\alpha\beta}(h)$ is due to the non-trivial 2-cocycles. For the two-dimensional systems without magnetic field, $f_{\alpha\beta}(h) \equiv 0$. For the case with magnetic field, in general $f_{\alpha\beta}(h)$ is nonzero.

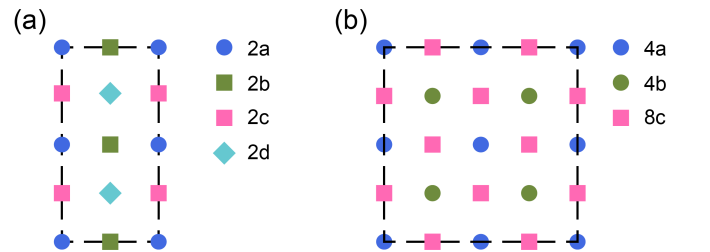


FIG. 4. (Color online) Wyckoff positions in a magnetic flux π for (a) the 2-by-1 unit cell for group $p2$ and (b) the 2-by-2 unit cell for the groups $p4$ and $p4/m'$. Each Wyckoff position is labelled by its multiplicity and a lowercase letter. The general Wyckoff position, whose site-symmetry group consists of only the identity, is not shown.

The phase factor $f_{\alpha\beta}(h)$ is the new ingredient that appears in a magnetic field and is a key result of the present work; it does not appear in the non-magnetic theory (for example, it does not appear in Eq. (6) in Ref. 11). This phase factor is gauge invariant because it results from the commutations between rotations and translations (see Appendix B). We briefly give two examples to show how this phase factor appears.

As a first example, consider the layer group $p1$ with a 2-by-2 unit cell, corresponding to π flux. Starting from a Wannier function centered at a general position $\mathbf{q} = (x, y)$, the coset representatives in Eq. (34) can be chosen as $g_1 = \{E|0\}$, $g_2 = T(\hat{\mathbf{x}})$, $g_3 = T(\hat{\mathbf{y}})$, $g_4 = T(\hat{\mathbf{x}})T(\hat{\mathbf{y}})$. Now consider the left-hand-side of Eq. (37) with $h = T(\hat{\mathbf{y}})$, $g_\alpha = T(\hat{\mathbf{x}})$. Then on the right-hand-side of Eq. (37), $g_\beta = T(\hat{\mathbf{x}})T(\hat{\mathbf{y}})$, $g = E$, and $\mathbf{t}_{\alpha\beta} = 0$. Since $T(\hat{\mathbf{y}})T(\hat{\mathbf{x}}) = e^{i\pi}T(\hat{\mathbf{x}})T(\hat{\mathbf{y}})$, $f_{\alpha\beta}(h) = \pi$.

As a second example, consider layer group $p4$ with a 2-by-2 unit cell, corresponding again to π flux. Starting from a Wannier function centered at $\mathbf{q} = (\frac{1}{2}, \frac{1}{2})$, the coset representatives in Eq. (34) can be chosen as $g_1 = \{E|0\}$, $g_2 = T(\hat{\mathbf{x}})$, $g_3 = T(\hat{\mathbf{y}})$, $g_4 = T(\hat{\mathbf{x}})T(\hat{\mathbf{y}})$. Now consider the left-hand-side of Eq. (37) with $h = C_4$, $g_\alpha = T(\hat{\mathbf{x}})$. The coset decomposition uniquely determines $g_\beta = T(\hat{\mathbf{x}})T(\hat{\mathbf{y}})$, $g = C_4(\frac{1}{2}, \frac{1}{2})$, and $\mathbf{t}_{\alpha\beta} = (-2, 0)$ on the right-hand-side of Eq. (37). Since $C_4T(\hat{\mathbf{x}}) = e^{i3\pi/4}\{E|(-2, 0)\}T(\hat{\mathbf{x}})T(\hat{\mathbf{y}})C_4(1/2, 1/2)$, the extra phase term $f_{\alpha\beta}(h) = 3\pi/4$.

As discussed at the start of Sec. IV, the set of Wannier functions centered at all \mathbf{q}_α form a basis for a band representation, which we denote ρ_G . Given a space group symmetry $h \in G$, Eq. (37) determines the matrix elements of $\rho_G(h)$ in the basis of Wannier functions defined in Eq. (36) by:

$$\rho_G(h)|W_{i\alpha}(\mathbf{r} - \mathbf{t})\rangle = e^{if_{\alpha\beta}(h)}[\rho(g)]_{ji}|W_{j\beta}(\mathbf{r} - R\mathbf{t} - \mathbf{t}_{\alpha\beta})\rangle \quad (38)$$

where R is the rotational part of h , $\rho(g)$ is the given representation defined in Eq. (35), $\mathbf{t}_{\alpha\beta}(h) = h\mathbf{q}_\alpha - \mathbf{q}_\beta$ and sum over $j = 1 \dots n_{\mathbf{q}}$ is implied.

Substituting the Fourier transformed Wannier functions,

$$|W_{j\beta}(\mathbf{r} - \mathbf{t})\rangle = \int d\mathbf{k} e^{i\mathbf{k}\cdot\mathbf{t}} |a_{j\beta}(\mathbf{k}, \mathbf{r})\rangle, \quad (39)$$

$$|a_{j\beta}(\mathbf{k}, \mathbf{r})\rangle = \sum_{\mathbf{t}} e^{-i\mathbf{k}\cdot\mathbf{t}} |W_{j\beta}(\mathbf{r} - \mathbf{t})\rangle, \quad (40)$$

into Eq. (38) yields

$$\rho_G(h)|a_{i\alpha}(\mathbf{k}, \mathbf{r})\rangle = e^{if_{\alpha\beta}(h) - iR\mathbf{k}\cdot\mathbf{t}_{\alpha\beta}} [\rho(g)]_{ji} |a_{j\beta}(R\mathbf{k}, \mathbf{r})\rangle \quad (41)$$

From Eq. (41), a representation of the little co-group (defined in Sec. III B) is determined from ρ_G by restricting each matrix $\rho_G(h \in \tilde{G}_{\mathbf{k}})$ to only the rows and column corresponding to Fourier-transformed Wannier functions at \mathbf{k} . The set of irreps obtained at all \mathbf{k} determines

the symmetry indicator following the procedure we introduced in Ref. 31, which is summarized in Appendix G.

We now derive the symmetry indicator classification for a few examples.

C. Examples

We apply our formalism of TQC in a magnetic flux to three magnetic layer groups with π flux: $p2$, $p4$, and $p4/m'$. In each case, we discuss the stable symmetry indicator classification; the derivations are in Appendix G. We further apply our formalism to derive the Chern number indicators in π flux for groups $p3$, $p4$ and $p6$ without spin-orbit coupling. They are shown in Appendix H.

1. $p2$

For layer group $p2$ with π flux, we choose a 2-by-1 magnetic unit cell, following the discussion in Sec. III A. The symmetry indicator has a \mathbb{Z}_4 classification. The indicator for a particular group of bands is

$$\text{index} = \#\Gamma_1 - \#\Gamma_2 + \#X_1 - \#X_2 + \#Y_1 - \#Y_2 + \#M_1 - \#M_2 - N \pmod{4} \quad (42)$$

where $\#\Pi_i$ indicates the number of times the irrep Π_i at the high symmetry point Π appears in the bands and $N = \#\Gamma_1 + \#\Gamma_2 = \#X_1 + \#X_2 = \#Y_1 + \#Y_2 = \#M_1 + \#M_2$ is the filling per magnetic unit cell.

This indicator Eq. (42) is exactly the same as the Chern number indicator Eq. (3) in Ref. 21 in the special case of π -flux and spinful electrons, i.e.,

$$e^{i\pi(C/q - \bar{\rho})} = (-)^{2SN} w_{C_2}^\Gamma w_{C_2}^Y w_{T(\hat{\mathbf{y}})C_2}^X w_{T(\hat{\mathbf{y}})C_2}^M \quad (43)$$

where at flux π , $q = 2$; $\bar{\rho} = N/2$ is the filling per non-magnetic primitive unit cell; $S = 1/2$ is the spin (angular momentum) quantum number; and w_g^Π is the product of eigenvalues of the symmetry g for all filled bands at momentum Π .

2. $p4$

For layer group $p4$ with π flux, we choose 2-by-2 unit cell, following the discussion in Sec. III A. The symmetry indicator has a \mathbb{Z}_8 classification. The indicators for a particular group of bands are determined by:

$$\text{index} = 2\#\Gamma_1 + 4\#\Gamma_2 - 2\#\Gamma_3 + \#M_1 + 3\#M_2 - 3\#M_3 - \#M_4 + 4\#X_1 \pmod{8} \quad (44)$$

To understand this indicator, we compare the new index to the symmetry indicator formula for Chern number in Ref. 22:

$$e^{i\frac{\pi}{2}C} = (-)^{2SN} w_{C_4}^\Gamma w_{C_2}^X w_{C_4}^M, \quad (45)$$

which, in terms of irreps, is given by (derivation in Appendix I)

$$C = 2N + \#\Gamma_1 + \#\Gamma_3 - \#\Gamma_2 - \#\Gamma_4 + 2(\#M_2 + \#M_4) \mod 4 \quad (46)$$

N is always an even integer due to the two-dimensional irreps (shown in Table III). We conclude

$$C = \text{index} \mod 4 \quad (47)$$

In fact this \mathbb{Z}_8 index is exactly the Chern number mod 8. This can be seen by considering a $\sqrt{2}$ -by- $\sqrt{2}$ unit cell which has lattice vectors $\mathbf{a}_1 = (1, 1)$, $\mathbf{a}_2 = (-1, 1)$; in this basis, Eq. (44) is identified as the \mathbb{Z}_8 Chern number indicator in Ref. 21.

3. $p4/m'$

For layer group $p4/m'$ with π flux, we choose 2-by-2 unit cell, following the discussion in Sec. III A. The symmetry indicator has a \mathbb{Z}_2 classification. The indicator for a particular group of bands is determined by:

$$\text{index} = N/4 \mod 2, \quad (48)$$

where $N/4 \equiv \bar{\rho}$ is the filling per original unit cell. Notice each band in this group is four-fold degenerate (see Table IV in Sec. III B), and hence $\bar{\rho} \in \mathbb{Z}$.

The group $p4/m'$ is generated by a four-fold rotation and the product of time-reversal and inversion symmetry \mathcal{TI} . As is well known, \mathcal{TI} prevents a non-vanishing Chern number [32] and the absence of \mathcal{T} prevents the existence of strong topological insulator [33]. Since \mathcal{T} and \mathcal{I} are not separately symmetries, there is no mirror symmetry and hence no mirror Chern number. Thus, our stable index is a new phase that only exists in systems with magnetic flux.

This phase is realized in the model we present in Sec. V. However, it does not realize an anomalous gapless boundary state because when the boundary is opened, the sublattice translation symmetries that protect the phase are broken.

V. APPLICATION TO A QUADRUPOLE INSULATOR

In this section, we apply our results to a model on the square lattice. At zero flux, this model is a quadrupole insulator that exhibits corner states. Since the symmetries that protect the corner states are preserved in the presence of a perpendicular magnetic field, the corner states must survive when magnetic flux is introduced. We use the formalism developed in the previous sections to verify the presence of corner states using symmetry indicators. Finally, we show that at a critical magnetic flux, the bulk gap closes and the corner states disappear, as shown in

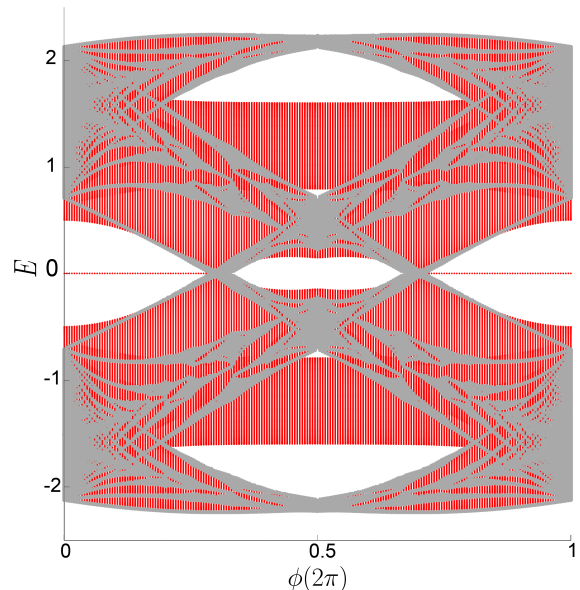


FIG. 5. (Color online) Hofstadter spectrum of the OAL model. The grey states are calculated with periodic boundary conditions and show the bulk gap closing at a critical flux. The red states are calculated with open boundary conditions and show the disappearance of the corner states upon bulk gap closure. The spectrum is computed for dimensions $L_x = 200$, $L_y = 10$ and parameters $\lambda = 1$, $\gamma = 0.5$.

the Hofstadter butterfly spectrum in Fig. 5. We use the symmetry indicators to verify that when the corner states disappear, the symmetry indicator vanishes.

Our results provide a new probe of the higher order topology in the model, i.e., the presence of a gap closing phase transition in the presence of a magnetic field, which may be easier to observe than probing the corner states directly.

A. Model

We study a model proposed by Wieder et al in Ref. 23 at zero flux that has the same momentum space Hamiltonian as the C_4 symmetric Bernevig-Benalcazar-Hughes (BBH) model which is at 4π flux per unit cell. [19, 20] This model was given as an example in Fig. 3 and Appendix A of Ref. 23. Yet the two models have some fundamental differences: while the BBH model has four atoms per unit cell and one orbital per atom, Wieder's model has one atom sitting at the origin of the unit cell and four orbitals per atom. Since the position of atoms in the unit cell will be important when we include magnetic flux, the two models have different Hofstadter spectra. Further, the BBH model describes spinless fermions, while Wieder's model describes fermions with spin-orbit coupling. As a result, the symmetry representations for

the two models are different.

In momentum space the Hamiltonian is

$$H(\mathbf{k}) = (v_m + t_1(\cos(k_x) + \cos(k_y)))\Gamma_3 + t_2(\cos(k_x) - \cos(k_y))\Gamma_4 + u \sin(k_x)\Gamma_1 + u \sin(k_y)\Gamma_2, \quad (49)$$

where $\Gamma_1 = \tau_y\sigma_y$, $\Gamma_2 = \tau_y\sigma_x$, $\Gamma_3 = \tau_z$, and $\Gamma_4 = \tau_x$. The Pauli matrices τ and σ together span the orbital space of each atom. In the limit $t_1 = t_2 = u/\sqrt{2} = \lambda/\sqrt{2}$ and $v_m = \sqrt{2}\gamma$, this Hamiltonian is equivalent to the BBH Hamiltonian after a basis change. In this section, we adopt these parameters and set $\lambda = 1$ and $\gamma = 0.5$ so that the system is a quadrupole insulator at zero flux.

The generators of the symmetries of this Hamiltonian take the matrix forms:

$$C_{4z} = \tau_z \left(\frac{\mathbb{I}_\sigma - \sigma_z}{2} \right), \quad (50)$$

$$M_x = \sigma_x, \quad (51)$$

$$\mathcal{TI} = \sigma_y\mathcal{K}, \quad (52)$$

where \mathcal{K} is the complex conjugation. There is also a chiral symmetry that anti-commutes with the Hamiltonian

$$\Gamma_5 = \tau_y\sigma_z \quad (53)$$

To incorporate the effect of a magnetic field, we need the real space Hamiltonian, given by:

$$H = \sum_{i,j \in \mathbb{Z}} \mathbf{t}_x c_{(i+1,j)}^\dagger c_{(i,j)} + \mathbf{t}_y c_{(i,j+1)}^\dagger c_{(i,j)} + h.c. + v_m \Gamma_3 c_{(i,j)}^\dagger c_{(i,j)} \quad (54)$$

where $\mathbf{t}_{x,y}$ are hopping matrices given by

$$\mathbf{t}_x = (t_1\Gamma_3 + t_2\Gamma_4)/2 - iu\Gamma_1/2 \quad (55)$$

$$\mathbf{t}_y = (t_1\Gamma_3 - t_2\Gamma_4)/2 - iu\Gamma_2/2 \quad (56)$$

When a magnetic field in the z -direction is turned on, the Hamiltonian in Eq. (54) requires the Peierls substitution [1]. Working in Landau gauge, $\mathbf{A}(x, y) = (-\phi y, 0)$ where $\phi = B$ is the flux per unit cell and the substitution is given by

$$c_{(i+1,j)}^\dagger c_{(i,j)} \mapsto e^{-i\phi j} c_{(i+1,j)}^\dagger c_{(i,j)} \quad (57)$$

$$c_{(i,j+1)}^\dagger c_{(i,j)} \mapsto c_{(i,j+1)}^\dagger c_{(i,j)} \quad (58)$$

The momentum space Hamiltonian at finite flux can be obtained by Fourier transforming Eq. (54) using the convention in Eqs. (23) and (24) when the flux is rational $\phi = 2\pi p/q$.

In Fig. 5, we numerically compute the Hofstadter spectrum for this model.

band index	1	2	3	4
irrep at Γ	$\Gamma_2\Gamma_3$	$\Gamma_1\Gamma_4$	$\Gamma_2\Gamma_3$	$\Gamma_1\Gamma_4$
irrep at X	X_1X_2	X_1X_2	X_1X_2	X_1X_2
irrep at M	M_2M_4	M_3M_3	M_1M_1	M_2M_4

TABLE V. Band representation of the four four-fold degenerate bands at π -flux. The ordering of band index is from lowest energy to highest energy, i.e., half-filling corresponds to filling bands 1 and 2. Each irrep $\Pi_i\Pi_j$ is four-dimensional and defined in Table IV.

B. Symmetry analysis

The model has a 2π periodicity in ϕ , the flux per unit cell. At zero flux and π -flux the system is invariant under the symmetry group $p4/m'mm$, while at other fluxes the symmetry group is $p4$. Using the formalism developed in this manuscript, we apply TQC in a magnetic field to compute the symmetry indicators at π flux. Indicators at other fluxes are discussed in Appendix J. Ultimately, we will show that the symmetry indicator at π flux corresponds to an absence of corner states, from which we deduce there must be a gap closing phase transition at a critical flux between zero and π .

At π -flux, the magnetic unit cell is 2-by-2 and the Brillouin zone is $[-\pi/2, \pi/2] \times [-\pi/2, \pi/2]$. According to Sec. III A, the four-fold rotation symmetry operators at $\Gamma = (0, 0)$ and $M = (\pi/2, \pi/2)$ are

$$D(C_{4z}, \Gamma) = \begin{pmatrix} 1 & & & \\ & 1 & & \\ & & & -1 \\ & & & \end{pmatrix} \otimes C_{4z}, \quad (59)$$

$$D(C_4, M) = \begin{pmatrix} 1 & & & \\ & -1 & & \\ & & & 1 \\ & & & \end{pmatrix} \otimes C_{4z}, \quad (60)$$

where the first matrix acts on the sublattice basis, and the C_{4z} matrix acts on the orbital basis as defined in Eq. (50). The magnetic translation symmetries at \mathbf{k} are implemented by

$$D(T(\hat{\mathbf{x}}), \mathbf{k}) = e^{ik_x} \begin{pmatrix} & 1 & & \\ 1 & & & \\ & & 1 & \\ & & & \end{pmatrix} \otimes \tau_0\sigma_0 \quad (61)$$

$$D(T(\hat{\mathbf{y}}), \mathbf{k}) = e^{ik_y} \begin{pmatrix} & & 1 & \\ & & & -1 \\ 1 & & & \\ & -1 & & \end{pmatrix} \otimes \tau_0\sigma_0, \quad (62)$$

where τ_0 and σ_0 are identity matrices.

The irreps of the occupied bands are listed in Table V. Each band is four-fold degenerate because $(\mathcal{TI})^2 = -1$ and $\{T(\hat{\mathbf{x}}), T(\hat{\mathbf{y}})\} = 0$, as explained in Appendix F. Using the computed irreps in Table V, the symmetry indicators are listed in Table VI.

band index	$n = 1, 4$	$n = 2, 3$	$1 \oplus 2$	$3 \oplus 4$
\mathbb{Z}_2 phase (Eq. (48))	1	1	0	0
$e_{4a} \bmod 8$			2	2
$e_{4b} \bmod 8$			0	0
$e_{8c} \bmod 4$			0	0
$e_{1a'} \bmod 4$	0	2	2	2
$e_{1b'} \bmod 4$	0	2	2	2
$e_{2c'} \bmod 2$	2	0	2	2

TABLE VI. Symmetry indicators at π -flux. The second column corresponds to each four-fold degenerate band individually, while the last two columns correspond to sums of bands. The second row shows the strong topological index in Eq. (48) is 1 mod 2 for each band, while for two occupied/empty bands the index is 0 mod 2. Since symmetric and exponentially localized Wannier functions exist for the two occupied or two empty bands, in the next three rows, $e_{\mathbf{q}}$ indicates the number of Wannier functions centered at the Wyckoff position \mathbf{q} , computed using Eqs. (G34) – (G36) in Appendix G. If the sublattice translation symmetry within each magnetic unit cell is broken, the number of Wannier functions centered at the indicated Wyckoff positions in the lower symmetry group are shown in Fig. 6.

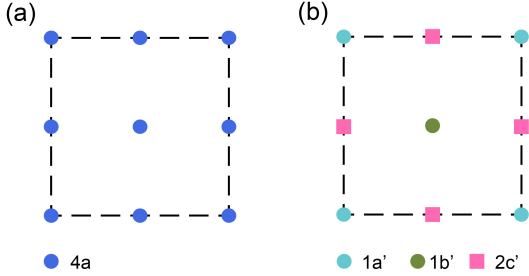


FIG. 6. (a) Wyckoff position $4a$ in 2-by-2 unit cell with space group G splits into (b) Wyckoff positions $1a'$, $1b'$, $2c'$ in the same unit cell with symmetry group $G/(\mathbb{T}/\mathbb{T}_M)$, i.e. no sublattice translations.

Below the gap at half filling, the two occupied bands together ($1 \oplus 2$ in Table VI) are topologically trivial. They admit symmetric exponentially localized Wannier functions located at the $4a$ Wyckoff position. Since the atoms are also at $4a$ Wyckoff position, there is no corner charge. This analysis agrees with the Hofstadter spectrum shown in Fig. 5.

Open boundary conditions break the lattice translation symmetries and, in particular, break the sublattice translation symmetries within the magnetic unit cell. Once the sublattice translation symmetries are broken, the little co-group (Eq. (32)) is identical to the non-magnetic case. Thus, the crystalline symmetry protected phases with open boundary condition should be labelled by the usual symmetry indicators in zero flux but with respect to the enlarged magnetic unit cell; these indicators are computed in Ref. 31. The results are shown in the lower half of Table VI. In this reduced symmetry group, the magnetic $4a$ Wyckoff position splits into positions: $1a' = (0, 0)$, $1b' = (1, 1)$, $2c' = (1, 0), (0, 1)$, as shown in

Fig. 6.

C. Corner states

The spectrum with periodic boundary condition has a gap at half filling at $\phi = 0$ and $\phi = \pi$. This gap closes at some ϕ^* between 0 and π as shown in Fig. 5. For the spectrum with open boundary condition, there are higher-order topological states when $-\phi^* < \phi < \phi^*$ that are corner localized. Due to the chiral symmetry (53), they are at zero energy in this model. The corner states can be understood by the non-zero quadrupole moment [19] or the non-zero filling anomaly [23, 31, 34, 35].

The corner states have four-fold degeneracy, consistent with the non-magnetic symmetry analysis in Refs. 31 and 36. The corner states with open boundary condition always come in a group of d states. This degeneracy d is determined by the point group of the finite system. Let w be the general Wyckoff position of the point group, with multiplicity n_w . Denote the site symmetry group G_w . It has only one irrep, $\rho(G_w)$. The degeneracy of corner states is [36]

$$d = \dim(\rho(G_w)) \times n_w \quad (63)$$

where $\dim(\rho(G_w)) = 2$ for spinful systems with time-reversal symmetry that squares to -1 , otherwise $\dim(\rho(G_w)) = 1$.

In the present case, at zero flux the system is invariant under the symmetry group $p4/m'mm$, while at any small flux the symmetry group reduces to $p4$. For $p4/m'mm$ and $p4$, the point groups of the finite size system are $4/m'mm$ and 4 respectively. Each has a general Wyckoff position w with $n_w = 4$ and $\dim(\rho(G_w)) = 1$; thus, Eq. (63) yields a degeneracy of 4 [36]. Since the degeneracy of corner states is the same for zero flux and finite flux, the corner states do not split when the magnetic flux is introduced (The chiral symmetry in this model pins the corner states to zero energy, but even in the absence of chiral symmetry, the nonzero filling anomaly will remain the same for $0 \leq \phi < \phi^*$.)

We have also shown from the symmetry indicators that at half filling and π flux, the system is in the trivial phase, without corner states. Thus, the corner states must terminate at $\phi = \phi^*$ by either a bulk or edge gap closing. There is indeed a bulk gap closing at flux ϕ^* as Fig. 5 shows. This is consistent with the Wannier centers of the occupied bands, which can be deduced from the symmetry indicators: the Wannier centers are at the $4b$ Wyckoff position at zero flux and the $4a$ Wyckoff position at π flux (see Table VI and Appendix J). Symmetries prevent four Wannier functions from moving continuously between the $4a$ and $4b$ positions [31, 37]. A discontinuous jump of the Wannier centers implies the bulk gap closes between zero and π flux.

In Appendix J we compute the symmetry indicator at intermediate flux $\phi = 2\pi/5 < \phi^*$ and $\phi = 4\pi/5 > \phi^*$ to verify that symmetry indicators are consistent with the

presence and absence of corner states between zero and π . In Appendix K we show that the presence and absence of corner states also agrees with the nested Wilson loops [19].

VI. CONCLUSION

In conclusion, we derived a general framework to apply TQC and the theory of symmetry indicators to crystalline systems at rational flux per unit cell. Applying our results to some simple examples at π flux revealed new symmetry indicators that did not appear at zero flux. Finally, the symmetry indicators enable us to study a quadrupole insulator at finite field, which reveals a gap closing topological-to-trivial phase transition as a function of magnetic field. Observing this phase transition could be particularly promising in moiré systems where higher flux is attainable for reasonable magnetic fields [38–41].

While preparing our work, we became aware of a related study [42], which gives criteria for when such a bulk gap closing at finite flux can be predicted from the band structure at zero flux. The two bulk gap closings between zero and $\Phi = 2\pi$ flux of our model in Sec. V are indicated by the real space invariant in Ref. 42.

We note that the Zeeman term is neglected in this manuscript. When the Zeeman term is present, the periodicity in the flux direction is broken. Thus there is no magnetic time-reversal symmetry or other mirror symmetries that flip magnetic flux. At large magnetic field where Zeeman term dominates, the two dimensional system must be in the trivial atomic limit where Wannier centers locate at the atom positions.

Our work is also restricted to a spatially constant magnetic field. It would be interesting to extend our results to

a spatially varying periodic magnetic field that maintains a commensurate flux per unit cell. This more general theory might be relevant to magnetically ordered crystals.

As a final note, we draw a connection between our results and the theory of phase space quantization, where one seeks a symmetric and exponentially localized Wannier basis that can continuously reduce to points in the classical phase space by setting the Planck constant $\hbar \rightarrow 0$ [43]. However, such a basis can never be found due to the Balian-Low theorem, which forbids the existence of exponentially localized translational symmetric basis for any single particle [44]. The magnetic Wannier functions in two dimensions share a similar translation group structure to the one-dimensional quantum phase space and the non-vanishing Chern number for any single magnetic band also forbids Wannierization [45], as we explain in Appendix L. Thus, there is an interesting open question: since in two dimensional magnetic systems, it is possible to find a Wannier basis for a group of bands, we conjecture that the continuous quantization of phase space may be realized by constructing Wannier functions for groups of particles.

VII. ACKNOWLEDGEMENTS

We acknowledge useful conversations with Andrei Bernevig, Aaron Dunbrack, Sayed Ali Akbar Ghorashi, Jonah Herzog-Arbeitman, and Oskar Vafek. We thank Jonah, Andrei, and their collaborators for sharing their unpublished manuscript.

Our manuscript is based upon work supported by the National Science Foundation under Grant No. DMR-1942447. The work was performed in part at the Aspen Center for Physics, which is supported by National Science Foundation grant PHY-1607611. J.C. also acknowledges the support of the Flatiron Institute, a division of the Simons Foundation.

-
- [1] D. R. Hofstadter, Energy levels and wave functions of bloch electrons in rational and irrational magnetic fields, *Physical Review B* **14**, 2239 (1976).
 - [2] J. Herzog-Arbeitman, Z.-D. Song, N. Regnault, and B. A. Bernevig, Hofstadter topology: noncrystalline topological materials at high flux, *Physical review letters* **125**, 236804 (2020).
 - [3] J. Wang and L. H. Santos, Classification of topological phase transitions and van hove singularity steering mechanism in graphene superlattices, *Physical Review Letters* **125**, 236805 (2020).
 - [4] Z.-W. Zuo, W. A. Benalcazar, Y. Liu, and C.-X. Liu, Topological phases of the dimerized hofstadter butterfly, *Journal of Physics D: Applied Physics* **54**, 414004 (2021).
 - [5] K. Asaga and T. Fukui, Boundary-obstructed topological phases of a massive Dirac fermion in a magnetic field, *Physical Review B* **102**, 155102 (2020).
 - [6] Y. Otaki and T. Fukui, Higher-order topological insulators in a magnetic field, *Physical Review B* **100**, 245108 (2019).
 - [7] Y. Zhang, N. Manjunath, G. Nambiar, and M. Barkeshli, Fractional disclination charge and discrete shift in the hofstadter butterfly, *arXiv preprint arXiv:2204.05320* (2022).
 - [8] B. Bradlyn, L. Elcoro, J. Cano, M. Vergniory, Z. Wang, C. Felser, M. Aroyo, and B. A. Bernevig, Topological quantum chemistry, *Nature* **547**, 298 (2017).
 - [9] M. Vergniory, L. Elcoro, Z. Wang, J. Cano, C. Felser, M. Aroyo, B. A. Bernevig, and B. Bradlyn, Graph theory data for topological quantum chemistry, *Physical Review E* **96**, 023310 (2017).
 - [10] L. Elcoro, B. Bradlyn, Z. Wang, M. G. Vergniory, J. Cano, C. Felser, B. A. Bernevig, D. Orobengoa, G. Flor, and M. I. Aroyo, Double crystallographic groups and their representations on the Bilbao Crystallographic Server, *Journal of Applied Crystallography* **50**, 1457 (2017).
 - [11] J. Cano, B. Bradlyn, Z. Wang, L. Elcoro, M. Vergniory, C. Felser, M. I. Aroyo, and B. A. Bernevig, Building blocks of topological quantum chemistry: Elementary

- band representations, *Physical Review B* **97**, 035139 (2018).
- [12] B. Bradlyn, L. Elcoro, M. Vergniory, J. Cano, Z. Wang, C. Felser, M. Aroyo, and B. A. Bernevig, Band connectivity for topological quantum chemistry: Band structures as a graph theory problem, *Physical Review B* **97**, 035138 (2018).
- [13] M. Vergniory, L. Elcoro, C. Felser, N. Regnault, B. A. Bernevig, and Z. Wang, A complete catalogue of high-quality topological materials, *Nature* **566**, 480 (2019).
- [14] J. Cano and B. Bradlyn, Band representations and topological quantum chemistry, *Annual Review of Condensed Matter Physics* **12**, 225 (2021).
- [15] L. Elcoro, B. J. Wieder, Z. Song, Y. Xu, B. Bradlyn, and B. A. Bernevig, Magnetic topological quantum chemistry, *Nature communications* **12**, 1 (2021).
- [16] H. C. Po, A. Vishwanath, and H. Watanabe, Symmetry-based indicators of band topology in the 230 space groups, *Nature communications* **8**, 1 (2017).
- [17] J. Zak, Magnetic translation group, *Physical Review* **134**, A1602 (1964).
- [18] J. Zak, Magnetic translation group. II. irreducible representations, *Physical Review* **134**, A1607 (1964).
- [19] W. A. Benalcazar, B. A. Bernevig, and T. L. Hughes, Electric multipole moments, topological multipole moment pumping, and chiral hinge states in crystalline insulators, *Physical Review B* **96**, 245115 (2017).
- [20] W. A. Benalcazar, B. A. Bernevig, and T. L. Hughes, Quantized electric multipole insulators, *Science* **357**, 61 (2017).
- [21] A. Matsugatani, Y. Ishiguro, K. Shiozaki, and H. Watanabe, Universal relation among the many-body chern number, rotation symmetry, and filling, *Physical Review Letters* **120**, 096601 (2018).
- [22] C. Fang, M. J. Gilbert, and B. A. Bernevig, Bulk topological invariants in noninteracting point group symmetric insulators, *Physical Review B* **86**, 115112 (2012).
- [23] B. J. Wieder, Z. Wang, J. Cano, X. Dai, L. M. Schoop, B. Bradlyn, and B. A. Bernevig, Strong and fragile topological Dirac semimetals with higher-order fermi arcs, *Nature communications* **11**, 1 (2020).
- [24] G. De Nittis and M. Lein, Exponentially localized wigner functions in periodic zero flux magnetic fields, *Journal of mathematical physics* **52**, 112103 (2011).
- [25] C. Bradley and A. Cracknell, *The mathematical theory of symmetry in solids: representation theory for point groups and space groups* (Oxford University Press, 2010).
- [26] J. Zak, Symmetry specification of bands in solids, *Phys. Rev. Lett.* **45**, 1025 (1980).
- [27] J. Zak, Band representations and symmetry types of bands in solids, *Phys. Rev. B* **23**, 2824 (1981).
- [28] L. Michel and J. Zak, Connectivity of energy bands in crystals, *Physical Review B* **59**, 5998 (1999).
- [29] L. Michel and J. Zak, Elementary energy bands in crystalline solids, *EPL (Europhysics Letters)* **50**, 519 (2000).
- [30] L. Michel and J. Zak, Elementary energy bands in crystals are connected, *Physics Reports* **341**, 377 (2001).
- [31] Y. Fang and J. Cano, Filling anomaly for general two- and three-dimensional C_4 symmetric lattices, *Phys. Rev. B* **103**, 165109 (2021).
- [32] B. A. Bernevig, Topological insulators and topological superconductors, in *Topological Insulators and Topological Superconductors* (Princeton university press, 2013).
- [33] L. Fu and C. L. Kane, Time reversal polarization and a z_2 adiabatic spin pump, *Physical Review B* **74**, 195312 (2006).
- [34] W. A. Benalcazar, T. Li, and T. L. Hughes, Quantization of fractional corner charge in c_n -symmetric higher-order topological crystalline insulators, *Physical Review B* **99**, 245151 (2019).
- [35] F. Schindler, M. Brzezińska, W. A. Benalcazar, M. Iraola, A. Bouhon, S. S. Tsirkin, M. G. Vergniory, and T. Neupert, Fractional corner charges in spin-orbit coupled crystals, *Phys. Rev. Research* **1**, 033074 (2019).
- [36] Y. Fang and J. Cano, Classification of Dirac points with higher-order fermi arcs, *Physical Review B* **104**, 245101 (2021).
- [37] Z. Song, Z. Fang, and C. Fang, (d-2)-dimensional edge states of rotation symmetry protected topological states, *Physical review letters* **119**, 246402 (2017).
- [38] I. Das, C. Shen, A. Jaoui, J. Herzog-Arbeitman, A. Chew, C.-W. Cho, K. Watanabe, T. Taniguchi, B. A. Piot, B. A. Bernevig, *et al.*, Observation of reentrant correlated insulators and interaction-driven fermi-surface reconstructions at one magnetic flux quantum per moiré unit cell in magic-angle twisted bilayer graphene, *Physical Review Letters* **128**, 217701 (2022).
- [39] Y. Xie, A. T. Pierce, J. M. Park, D. E. Parker, E. Khalaf, P. Ledwith, Y. Cao, S. H. Lee, S. Chen, P. R. Forrester, *et al.*, Fractional chern insulators in magic-angle twisted bilayer graphene, *Nature* **600**, 439 (2021).
- [40] A. T. Pierce, Y. Xie, J. M. Park, E. Khalaf, S. H. Lee, Y. Cao, D. E. Parker, P. R. Forrester, S. Chen, K. Watanabe, *et al.*, Unconventional sequence of correlated chern insulators in magic-angle twisted bilayer graphene, *Nature Physics* **17**, 1210 (2021).
- [41] J. Yu, B. A. Foutty, Z. Han, M. E. Barber, Y. Schattner, K. Watanabe, T. Taniguchi, P. Phillips, Z.-X. Shen, S. A. Kivelson, *et al.*, Correlated hofstadter spectrum and flavour phase diagram in magic-angle twisted bilayer graphene, *Nature Physics* , 1 (2022).
- [42] J. Herzog-Arbeitman, Z.-D. Song, L. Elcoro, and B. A. Bernevig, Hofstadter topology with real space invariants and reentrant projective symmetries, *arXiv preprint arXiv:2209.10559* (2022).
- [43] J. Von Neumann, Mathematical foundations of quantum mechanics, in *Mathematical Foundations of Quantum Mechanics* (Princeton university press, 2018).
- [44] J. J. Benedetto, C. Heil, and D. F. Walnut, Differentiation and the balian-low theorem, *Journal of Fourier Analysis and Applications* **1**, 355 (1994).
- [45] J. Zak, Balian-low theorem for Landau levels, *Physical review letters* **79**, 533 (1997).
- [46] J. Herzog-Arbeitman, A. Chew, and B. A. Bernevig, Magnetic bloch theorem and reentrant flat bands in twisted bilayer graphene at 2π flux, *arXiv preprint arXiv:2206.07717* (2022).
- [47] D. Gorenstein, *Finite groups*, Vol. 301 (American Mathematical Soc., 2007).
- [48] Z.-D. Song, L. Elcoro, Y.-F. Xu, N. Regnault, and B. A. Bernevig, Fragile phases as affine monoids: classification and material examples, *Physical Review X* **10**, 031001 (2020).
- [49] Z.-D. Song, L. Elcoro, and B. A. Bernevig, Twisted bulk-boundary correspondence of fragile topology, *Science* **367**, 794 (2020).
- [50] Z. Song, T. Zhang, Z. Fang, and C. Fang, Quantitative mappings between symmetry and topology in solids, *Nature*

- ture communications **9**, 1 (2018).
- [51] H. Watanabe and S. Ono, Corner charge and bulk multipole moment in periodic systems, *Physical Review B* **102**, 165120 (2020).
 - [52] A. Alexandradinata, X. Dai, and B. A. Bernevig, Wilson-loop characterization of inversion-symmetric topological insulators, *Physical Review B* **89**, 155114 (2014).
 - [53] B. Bradlyn, Z. Wang, J. Cano, and B. A. Bernevig, Disconnected elementary band representations, fragile topology, and wilson loops as topological indices: An example on the triangular lattice, *Physical Review B* **99**, 045140 (2019).
 - [54] R. Resta and D. Vanderbilt, Theory of polarization: a modern approach, in *Physics of Ferroelectrics* (Springer, 2007) pp. 31–68.
 - [55] W. A. Wheeler, L. K. Wagner, and T. L. Hughes, Many-body electric multipole operators in extended systems, *Physical Review B* **100**, 245135 (2019).
 - [56] G. Battle, Heisenberg proof of the balian-low theorem, *Letters in Mathematical Physics* **15**, 175 (1988).
 - [57] M. Moscolari and G. Panati, Symmetry and localization for magnetic Schroedinger operators: Landau levels, Gabor frames and all that, *Acta Applicandae Mathematicae* **162**, 105 (2019).
 - [58] P. Streda, Theory of quantised hall conductivity in two dimensions, *Journal of Physics C: Solid State Physics* **15**, L717 (1982).
 - [59] D. Thouless, Wannier functions for magnetic sub-bands, *Journal of Physics C: Solid State Physics* **17**, L325 (1984).

Appendix A: Derivation of λ_g in Eq. (6)

In this appendix, we derive Eq. (6) starting from Eq. (5), which we rewrite here for convenience:

$$\int_{\mathbf{r}_1}^{\mathbf{r}_2} \mathbf{A}(\mathbf{r}) \cdot d\mathbf{r} + \int_{\hat{g}\mathbf{r}_1}^{\hat{g}\mathbf{r}_2} \nabla \lambda(\mathbf{r}') \cdot d\mathbf{r}' = \int_{\hat{g}\mathbf{r}_1}^{\hat{g}\mathbf{r}_2} \mathbf{A}(\mathbf{r}') \cdot d\mathbf{r}' \quad (\text{A1})$$

Substituting $\mathbf{r} = \hat{g}^{-1}\mathbf{r}'$ in the first term on the left side of Eq. (A1) yields

$$\begin{aligned} \int_{\mathbf{r}_1}^{\mathbf{r}_2} \mathbf{A}(\mathbf{r}) \cdot d\mathbf{r} &= \int_{\hat{g}\mathbf{r}_1}^{\hat{g}\mathbf{r}_2} \mathbf{A}(\hat{g}^{-1}\mathbf{r}') \cdot d(\hat{g}^{-1}\mathbf{r}') \\ &= \int_{\hat{g}\mathbf{r}_1}^{\hat{g}\mathbf{r}_2} \mathbf{A}(\hat{g}^{-1}\mathbf{r}') \cdot R_g^{-1} d\mathbf{r}' \\ &= \int_{\hat{g}\mathbf{r}_1}^{\hat{g}\mathbf{r}_2} R_g \mathbf{A}(\hat{g}^{-1}\mathbf{r}') \cdot d\mathbf{r}' \end{aligned} \quad (\text{A2})$$

In the second equality we have defined the rotation R_g by the action $\hat{g} : \mathbf{r} \mapsto R_g \mathbf{r} + \tau_g$, from which it follows that $\hat{g}^{-1} : \mathbf{r} \mapsto R_g^{-1}\mathbf{r} - R_g^{-1}\tau_g$, and, consequently, $d(\hat{g}^{-1}\mathbf{r}') = R_g^{-1}d\mathbf{r}'$, since $d(R_g^{-1}\tau_g) = 0$. Eqs. (A1) and (A2) together are exactly the integral form of Eq. (6).

Appendix B: Gauge invariant commutation relations between translation and rotation operators

In this Appendix, we derive the commutation relations for magnetic rotation and translation symmetry operators in real space. We show these relations are gauge invariant. The results are used in Secs. II and IV and Appendix F.

We denote an n -fold magnetic rotation operator centered about (\bar{x}_1, \bar{x}_2) as $C_n(\bar{x}_1, \bar{x}_2)$. For rotations about the origin, we simplify the notation by dropping the argument (\bar{x}_1, \bar{x}_2) , i.e., $C_n \equiv C_n(\bar{x}_1 = 0, \bar{x}_2 = 0)$. We define $C_n(\bar{x}, \bar{y})$ by conjugating magnetic translation operators with C_n

$$C_n(\bar{x}_1, \bar{x}_2) \equiv T(\bar{x}_1 \hat{\mathbf{x}}_1 + \bar{x}_2 \hat{\mathbf{x}}_2) C_n T(-\bar{x}_1 \hat{\mathbf{x}}_1 - \bar{x}_2 \hat{\mathbf{x}}_2) \quad (\text{B1})$$

where $\hat{\mathbf{x}}_1$ and $\hat{\mathbf{x}}_2$ are unit vectors in the x_1 and x_2 directions. This definition is a general form for any gauge choice of vector potential. In this definition $(C_n(\bar{x}_1, \bar{x}_2))^n = C_n^n$ is the identity. The definition is independent of the ordering of translations. For example,

$$\begin{aligned} C_n(\bar{x}_1, \bar{x}_2) &= T(\bar{x}_2 \hat{\mathbf{x}}_2) T(\bar{x}_1 \hat{\mathbf{x}}_1) C_n T(-\bar{x}_1 \hat{\mathbf{x}}_1) T(-\bar{x}_2 \hat{\mathbf{x}}_2) \\ &= T(\bar{x}_1 \hat{\mathbf{x}}_1) T(\bar{x}_2 \hat{\mathbf{x}}_2) C_n T(-\bar{x}_2 \hat{\mathbf{x}}_2) T(-\bar{x}_1 \hat{\mathbf{x}}_1) \end{aligned}$$

We now derive commutation relations between the magnetic rotations and translations. First, we derive a gauge invariant commutation relation between a translation $T(\mathbf{a})$ and C_n ,

$$C_n T(\mathbf{a}) = T(R_n \mathbf{a}) C_n, \quad (\text{B2})$$

which is the same as the commutation relation in zero field. We now prove Eq. (B2); Ref. 46 gives a different proof of Eq. (B2).

Eq. (9) provides explicit operator forms for C_n and $T(\mathbf{a})$:

$$C_n = \sum_{\mathbf{x}} e^{i\lambda_{C_n}(\mathbf{R}_n \mathbf{x})} c_{\mathbf{R}_n \mathbf{x}}^\dagger c_{\mathbf{x}} \quad (\text{B3})$$

$$T(\mathbf{a}) = \sum_{\mathbf{x}} e^{i\lambda_{T(\mathbf{a})}(\mathbf{x} + \mathbf{a})} c_{\mathbf{x} + \mathbf{a}}^\dagger c_{\mathbf{x}} \quad (\text{B4})$$

The gauge dependence of the operators are encoded in the definition of λ_g . The explicit expression of λ_{C_n} and $\lambda_{T(\mathbf{a})}$ from Eqs. (6) and (7) in our definition are

$$\begin{aligned} \lambda_{C_n}(\mathbf{x}) &= \int_{\mathbf{r}_0}^{\mathbf{x}} \mathbf{A}(\mathbf{x}') - R_n \mathbf{A}(R_n^{-1} \mathbf{x}') \cdot d\mathbf{x}' \\ &= \left[\int_{\mathbf{r}_0}^{\mathbf{x}} - \int_{R_n^{-1} \mathbf{r}_0}^{R_n^{-1} \mathbf{x}} \right] \mathbf{A}(\mathbf{x}') \cdot d\mathbf{x}' \end{aligned} \quad (\text{B5})$$

$$\lambda_{T(\mathbf{a})}(\mathbf{x}) = \int_{\mathbf{x} - \mathbf{a}}^{\mathbf{x}} \mathbf{A}(\mathbf{x}') \cdot d\mathbf{x}' + \mathbf{B} \cdot \mathbf{a} \times \mathbf{x} \quad (\text{B6})$$

where \mathbf{r}_0 is a reference point that will cancel below.

Plugging into Eq. (B2) and considering the action on single particle states, the equation holds when the phase terms on both sides are equal, i.e.,

$$\begin{aligned} \lambda_{C_n}(R_n(\mathbf{x} + \mathbf{a})) + \lambda_{T(\mathbf{a})}(\mathbf{x} + \mathbf{a}) \\ = \lambda_{T(R_n \mathbf{a})}(R_n(\mathbf{x} + \mathbf{a})) + \lambda_{C_n}(R_n \mathbf{x}). \end{aligned} \quad (\text{B7})$$

Applying Eq. (B5) yields

$$\begin{aligned} \lambda_{C_n}(R_n(\mathbf{x} + \mathbf{a})) - \lambda_{C_n}(R_n \mathbf{x}) \\ = \left[\int_{\mathbf{r}_0}^{R_n(\mathbf{x} + \mathbf{a})} - \int_{R_n^{-1} \mathbf{r}_0}^{\mathbf{x} + \mathbf{a}} - \int_{\mathbf{r}_0}^{R_n \mathbf{x}} + \int_{R_n^{-1} \mathbf{r}_0}^{\mathbf{x}} \right] \mathbf{A}(\mathbf{x}') \cdot d\mathbf{x}' \\ = \left[\int_{R_n \mathbf{x}}^{R_n(\mathbf{x} + \mathbf{a})} + \oint_{R_n \mathcal{C}} - \int_{\mathbf{x}}^{\mathbf{x} + \mathbf{a}} - \oint_{\mathcal{C}} \right] \mathbf{A}(\mathbf{x}) \cdot d\mathbf{r} \\ = \left[\int_{R_n \mathbf{x}}^{R_n(\mathbf{x} + \mathbf{a})} - \int_{\mathbf{x}}^{\mathbf{x} + \mathbf{a}} \right] \mathbf{A}(\mathbf{x}) \cdot d\mathbf{r}, \end{aligned} \quad (\text{B8})$$

where the path \mathcal{C} is a triangle whose vertices are $R_n^{-1} \mathbf{r}_0$, \mathbf{x} , $\mathbf{x} + \mathbf{a}$. The last equality follows because the two closed loops enclose the same amount of flux. Then applying Eq. (B6) yields

$$\begin{aligned} \lambda_{T(R_n \mathbf{a})}(R_n(\mathbf{x} + \mathbf{a})) - \lambda_{T(\mathbf{a})}(\mathbf{x} + \mathbf{a}) \\ = \left[\int_{R_n \mathbf{x}}^{R_n(\mathbf{x} + \mathbf{a})} - \int_{\mathbf{x}}^{\mathbf{x} + \mathbf{a}} \right] \mathbf{A}(\mathbf{x}) \cdot d\mathbf{r}. \end{aligned} \quad (\text{B9})$$

The two expressions are equal, proving Eq. (B2).

Combined with the gauge invariant relation for magnetic translations (Eq. (16) in the main text),

$$T(\mathbf{a}_1) T(\mathbf{a}_2) = T(\mathbf{a}_1 + \mathbf{a}_2) e^{\frac{i}{2} \mathbf{B} \cdot (\mathbf{a}_1 \times \mathbf{a}_2)}, \quad (\text{B10})$$

Eq. (B2) implies that the phases that appear in the commutation relations between $C_n(\bar{x}_1, \bar{x}_2)$ and $T(\mathbf{a})$ are all gauge invariant. For example, for two-fold and four-fold magnetic rotations on a square lattice

$$\begin{aligned} C_2(\bar{x}, \bar{y})T(\Delta\hat{\mathbf{x}}) &= T(-\Delta\hat{\mathbf{x}})C_2(\bar{x}, \bar{y})e^{-2iB\Delta\bar{y}} \\ C_2(\bar{x}, \bar{y})T(\Delta\hat{\mathbf{y}}) &= T(-\Delta\hat{\mathbf{y}})C_2(\bar{x}, \bar{y})e^{2iB\Delta\bar{x}} \\ C_4(\bar{x}, \bar{y})T(\Delta\hat{\mathbf{x}}) &= T(\Delta\hat{\mathbf{y}})C_4(\bar{x}, \bar{y})e^{-iB\Delta(\bar{x}+\bar{y})} \\ C_4(\bar{x}, \bar{y})T(\Delta\hat{\mathbf{y}}) &= T(-\Delta\hat{\mathbf{x}})C_4(\bar{x}, \bar{y})e^{iB\Delta(\bar{x}-\bar{y})} \end{aligned} \quad (\text{B11})$$

and

$$\begin{aligned} C_2(\bar{x}_1, \bar{y}_1)C_2(\bar{x}_2, \bar{y}_2) &= C_2(-\bar{x}_2, -\bar{y}_2)C_2(-\bar{x}_1, -\bar{y}_1) \\ &\quad e^{4iB(\bar{x}_1\bar{y}_1 - \bar{x}_2\bar{y}_2 + \bar{x}_2\bar{y}_1 - \bar{x}_1\bar{y}_2)} \\ C_4(\bar{x}_1, \bar{y}_1)C_4(\bar{x}_2, \bar{y}_2) &= C_4(-\bar{y}_2, \bar{x}_2)C_4(\bar{y}_1, -\bar{x}_1) \\ &\quad e^{iB((\bar{x}_1+\bar{x}_2)^2 - (\bar{y}_1-\bar{y}_2)^2)} \end{aligned} \quad (\text{B12})$$

These relations are used when we study irreducible representations in Sec. III B and topological quantum chemistry in Sec. IV.

Appendix C: Projective representation

In general, a projective representation ρ of a group G satisfies

$$\rho(g_1)\rho(g_2) = \omega(g_1, g_2)\rho(g_1g_2) \quad (\text{C1})$$

for all $g_1, g_2 \in G$, where $\omega(g_1, g_2)$ is called the 2-cocycle (or Schur multiplier, or factor system). When $\omega(g_1, g_2) \equiv 1$, the representation is an ordinary linear representation.

Under a gauge transformation of ρ by $\rho'(g) = f(g)\rho(g)$, 2-cocycles satisfy the cocycle condition $\omega'(g_1, g_2) = f(g_1g_2)f(g_1)^{-1}f(g_2)^{-1}\omega(g_1, g_2)$, which defines an equivalence class $[\omega(g_1, g_2)]$ of cocycles. The classification of the equivalence classes is determined by the group cohomology.

In the remaining part of this section, we explain the standard way to derive irreducible projective representations through the group extension. The magnetic symmetries can be viewed as projective representations of the non-magnetic symmetries. These projective representations are projected from the ordinary representations of a larger group that can be described as a group extension of the non-magnetic group. For example, the continuous magnetic translations form the Heisenberg group $Heis$. It is extended from the non-magnetic translations \mathbb{R}^2 by the abelian group $U(1)$. There are many irreducible representations of $Heis$, but only some of them are compatible with the 2-cocycles, which are the phases due to gauge transformations of the magnetic symmetries. For example, the trivial irreducible representation is not compatible with the particular 2-cocycles.

We now describe the group extension for the translation symmetries on a square lattice as a concrete example. Consider a model with only nearest neighbor

hopping. Then the phase introduced by the magnetic translations in Eq. (15) with commensurate magnetic flux $\phi = 2\pi p/q$ belongs to \mathbb{Z}_q . We first consider the extension of full translation group $\mathbb{T} = \mathbb{Z} \times \mathbb{Z}$ by \mathbb{Z}_q . This real space Heisenberg group is defined by the central group extension, which is a short exact sequence

$$1 \longrightarrow \mathbb{Z}_q \xrightarrow{i} Heis \xrightarrow{\pi} \mathbb{Z} \times \mathbb{Z} \longrightarrow 1 \quad (\text{C2})$$

where each arrow is a group homomorphism and $\text{im}(i) = \ker(\pi)$. Next we consider the momentum space Heisenberg group $Heis_k$ (for the q -by- q unit cell), which is the sublattice translation group \mathbb{T}/\mathbb{T}_M extended by \mathbb{Z}_q . Its defining central group extension is

$$1 \longrightarrow \mathbb{Z}_q \xrightarrow{i} Heis_k \xrightarrow{\pi} \mathbb{Z}_q \times \mathbb{Z}_q \longrightarrow 1 \quad (\text{C3})$$

It can be shown that this $Heis_k$ is an extra special group of order q^3 . It has q^2 1-dimensional irreducible representations and $q-1$ q -dimensional irreducible representations [47]. The abelian group \mathbb{Z}_q acts trivially on the 1-dimensional irreps. Thus, the projective representations are projected from the q -dimensional representations. Therefore, the momentum space states satisfying magnetic translation symmetries are q -fold degenerate. For example, at π flux, $Heis_k$ is isomorphic to the group D_4 and the irreducible projective representation of translations $\mathbb{Z}_2 \times \mathbb{Z}_2$ is projected from the only two-dimensional irreducible representation E of D_4 .

For more complicated cases with magnetic rotation symmetries, in principle one can use the same formalism to get the corresponding extended group and the irreducible projective representations of the unextended symmetry group. However, practically it is easier to derive the irreducible projective representations by studying the (anti-)commutation relations as shown in Appendix F.

Appendix D: Triangular lattice symmetries in a magnetic field

The Landau gauge in triangular and hexagonal lattices is defined differently than for the square lattice. Therefore, we discuss the magnetic symmetries of these lattices separately here.

We consider the lattice vectors $\mathbf{a}_1 = (1, 0)$, $\mathbf{a}_2 = (\frac{1}{2}, \frac{\sqrt{3}}{2})$ in Cartesian coordinates. The reciprocal lattice vectors are $\mathbf{b}_1 = (1, -1/\sqrt{3})$, $\mathbf{b}_2 = (0, 2/\sqrt{3})$ in Cartesian coordinates, where $\mathbf{a}_i \cdot \mathbf{b}_j = \delta_{ij}$. The vector potential for the magnetic field in Landau gauge is $\mathbf{A}(\mathbf{r}) = -\phi\mathbf{b}_1(\mathbf{b}_2 \cdot \mathbf{r})$, where ϕ is the flux per primitive unit cell. It is helpful to note the gradient in these coordinates is $\nabla = \mathbf{b}_1\partial_{r_1} + \mathbf{b}_2\partial_{r_2}$.

From Eq. (6) we can compute the gauge transformation terms $\lambda(r_1, r_2)$, where $\mathbf{r} = r_1\mathbf{a}_1 + r_2\mathbf{a}_2$. The results for several spatial symmetries \hat{g} compatible with the triangular lattice are summarized in Table VII.

g	$T(\Delta_1 \hat{\mathbf{x}}_1)$	$T(\Delta_2 \hat{\mathbf{x}}_2)$	$C_2(\bar{r}_1, \bar{r}_2)$	$C_6(\bar{r}_1, \bar{r}_2)$	$C_3(\bar{r}_1, \bar{r}_2)$
$\hat{g} = \{R_g \tau_g\}$	$\{0 (\Delta_1, 0)\}$	$\{0 (0, \Delta_2)\}$	$\{\hat{C}_2 (2\bar{r}_1, 2\bar{r}_2)\}$	$\{\hat{C}_6 (\bar{r}_1 + \bar{r}_2, -\bar{r}_1)\}$	$\{\hat{C}_3 (2\bar{r}_1 + \bar{r}_2, \bar{r}_2 - \bar{r}_1)\}$
$\lambda(r_1, r_2)$	0	$-\phi \Delta_2 r_1$	$-2\phi \bar{r}_2(r_1 - \bar{r}_1)$	$-\phi((r_1 - \bar{r}_1)(r_2 - \bar{r}_2) + \frac{(r_1 - \bar{r}_1)^2}{2}) + \phi \bar{r}_2(r_2 - \bar{r}_2)$	$-\phi((r_1 - \bar{r}_1)(r_2 - \bar{r}_2) + \frac{(r_2 - \bar{r}_2)^2}{2}) - \phi \bar{r}_2((r_1 - \bar{r}_1) - (r_2 - \bar{r}_2))$

TABLE VII. The gauge transformation $\lambda_g(x, y)$ for symmetries of the six-fold symmetric triangular lattice in Landau gauge. For each symmetry g in the first row, the second row lists the symmetry in the notation $\{R_g | \tau_g\}$ and the third row provides λ_g from Eq. (6).

Appendix E: Equivalent representations for the q -by-1 and q -by- q unit cells

In this appendix, we argue that the symmetry operators for the q -by-1 and q -by- q unit cells form equivalent $q^2 \times q^2$ -dimensional representations. We study C_4 and $T(\hat{\mathbf{y}})$ as examples.

1. q -by-1 unit cell

As shown in Sec. III A 1, in the q -by-1 unit cell the C_4 symmetry mixes a Bloch eigenstate at momentum (k_x, k_y) into a linear combination of eigenstates at momenta $(k_y + 2\pi l/q, -k_x)$, $l = 0, 1, \dots, q-1$. Each momentum can be classified by the number of other momenta it mixes with under C_4 : a generic \mathbf{k} mixes into $4q$ distinct momenta; $(\pi, 0)$ mixes into $2q$ momenta (including $(0, \pi/q)$); and $(0, 0)$ or $(\pi/q, \pi/q)$ mix into q distinct momenta.

We now compute the symmetry operators for the high-symmetry momenta, $(0, 0)$ and $(\pi/q, \pi/q)$. The $T(\hat{\mathbf{y}})$ and C_4 symmetries will be implemented by a $q^2 \times q^2$ matrix: the first factor of q comes from the q original unit cells in the magnetic unit cell, while the second factor comes from q different momenta that mix into each other under C_4 . Specifically, following Eqs. (25) and (26), at the high-symmetry points $\mathbf{k} = \Gamma$ or M , we choose the basis $\{c_{(l\phi, 0), j}^\dagger | 0\rangle\}$ or $\{c_{(\pi/q + l\phi, \pi/q), j}^\dagger | 0\rangle\}$, respectively, where $l, j = 0, 1, \dots, q-1$.

As a concrete example, we write the matrix form of the symmetry operators at $\phi = \pi$ flux, i.e., $q = 2$. A symmetry operator g defined in the above basis takes the general form

$$g = \frac{q}{(2\pi)^2} \int_0^{\frac{2\pi}{q}} \int_0^{\frac{2\pi}{q}} d\mathbf{k} \sum_{l, j, l', j'=0,1} c_{\mathbf{k}, l, j}^\dagger D(g, \mathbf{k})_{l, j; l', j'} c_{\mathbf{k}, l', j'} \quad (\text{E1})$$

where $c_{\mathbf{k}, l, j} = c_{\mathbf{k} + l(2\pi/q, 0), j}$ and $D(g, \mathbf{k})_{l, j; l', j'}$ is a 4×4 matrix. (This form does not apply at momenta other than $(0, 0)$ or $(\pi/2, \pi/2)$; at other momenta the C_4 symmetry requires a larger matrix.)

Taking the specific symmetries $g = T(\hat{\mathbf{y}})$ or C_4 ,

$$D(T(\hat{\mathbf{y}}), \mathbf{k}) = e^{ik_y} \begin{pmatrix} & & 1 \\ & 1 & \\ 1 & & \end{pmatrix}, \quad (\text{E2})$$

whose eigenvalues are $e^{ik_y} \{+1, +1, -1, -1\}$;

$$D(C_4, \Gamma) = \frac{1}{2} \begin{pmatrix} 1 & 1 & 1 & 1 \\ 1 & -1 & -1 & 1 \\ 1 & -1 & 1 & -1 \\ 1 & 1 & -1 & -1 \end{pmatrix}, \quad (\text{E3})$$

whose eigenvalues are $\{+1, +1, -1, -1\}$; and

$$D(C_4, (\pi/2, \pi/2)) = \frac{1}{2} \begin{pmatrix} 1 & -i & 1 & -i \\ -i & 1 & i & -1 \\ 1 & i & 1 & i \\ -i & -1 & i & 1 \end{pmatrix}, \quad (\text{E4})$$

whose eigenvalues are $\{+1, +1, +i, -i\}$.

2. q -by- q unit cell

For the q -by- q unit cell, the C_4 operator behaves similar to the non-magnetic case, in that it mixes each Bloch wave function into a single other Bloch wave function. The highest symmetry points are $\Gamma = (0, 0)$ and $M = (\pi/q, \pi/q)$.

As in the previous section, we consider the flux $\phi = \pi$ as an example. An operator g takes the general form

$$g = \left(\frac{q}{2\pi}\right)^2 \int d\mathbf{k} \sum_{j_x, j_y, j'_x, j'_y} c_{\mathbf{k}, j_x, j_y}^\dagger D(g, \mathbf{k})_{j_x, j_y; j'_x, j'_y} c_{\mathbf{k}, j'_x, j'_y} \quad (\text{E5})$$

This form of the matrix representation $D(g, \mathbf{k})$ is valid for $T(\hat{\mathbf{y}})$ at any \mathbf{k} and for C_4 at $\Gamma = (0, 0)$ and $M = (\pi/q, \pi/q)$. From Eqs. (29) and (30),

$$D(T(\hat{\mathbf{y}}), \mathbf{k}) = e^{ik_y} \begin{pmatrix} & & 1 \\ & & -1 \\ 1 & & \\ & -1 & \end{pmatrix} \quad (\text{E6})$$

whose eigenvalues are $e^{ik_y} \{+1, +1, -1, -1\}$;

$$D(C_4, (0, 0)) = \begin{pmatrix} 1 & & & \\ & 1 & & \\ & & 1 & \\ & & & -1 \end{pmatrix}, \quad (\text{E7})$$

whose eigenvalues are $\{+1, +1, -1, -1\}$; and

$$D(C_4, (\pi/2, \pi/2)) = \begin{pmatrix} 1 & & & \\ & -1 & & \\ & & 1 & \\ & & & 1 \end{pmatrix}, \quad (\text{E8})$$

whose eigenvalues are $\{+1, +1, +i, -i\}$.

These eigenvalues are identical to the eigenvalues of the symmetry operators derived for the q -by-1 unit cell in Eqs. (E2), (E3) and (E4), which implies that the representations of the symmetry operators are the same for a q -by-1 unit cell and a q -by- q unit cell.

In conclusion: the two natural choices of magnetic unit cell yield unitarily equivalent symmetry representations, but the q -by- q unit cell allows the symmetry operators to act in a more familiar way because their action on \mathbf{k} is identical to that in zero field.

Appendix F: Irreps at high symmetry momenta for $p2, p4, p4/m'$

The irreps of little co-groups at high symmetry momenta for $p2, p4$ and $p4/m'$ with π flux are calculated in detail in this section. The results are summarized in Tables II, III, and IV in Sec. III B.

For simplicity, we denote $T_x \equiv T(\hat{\mathbf{x}})$, $T_y \equiv T(\hat{\mathbf{y}})$ in this section.

In this appendix, we will repeatedly use the gauge invariant commutation relation

$$C_n T(\mathbf{a}) = T(R_n \mathbf{a}) C_n \quad (\text{F1})$$

which is derived in Appendix B and

$$T_x T_y = T_y T_x e^{i\phi} = -T_y T_x \quad (\text{F2})$$

which is a consequence of the Aharonov-Bohm phase. We will also use $T_x^2 = e^{2ik_x}$, $T_y^2 = e^{2ik_y}$ to derive the (anti-)commutation relations of rotation and translation symmetries.

1. $p2$

We first study the $p2$ with $\phi = \pi$ and a 2-by-1 unit cell. The magnetic lattice translation group is $\mathbb{T}_M = \{(n_1, 2n_2) | n_1, n_2 \in \mathbb{Z}\}$. The little co-group is a subgroup of $p2/\mathbb{T}_M$, which is generated by C_2 and T_y symmetries.

For the 2-by-1 unit cell, the Brillouin zone is $[-\pi, \pi] \times [-\pi/2, \pi/2]$. In momentum space, T_y maps $(k_x, k_y) \mapsto (k_x + \pi, k_y)$ because Eq. (F2) implies

$$\begin{aligned} T_x T_y |k_x, k_y\rangle &= -T_y T_x |k_x, k_y\rangle \\ &= e^{i(k_x + \pi)} T_y |k_x, k_y\rangle \end{aligned} \quad (\text{F3})$$

Therefore, given a Bloch wave function $|0, 0; \xi\rangle$ at $(0, 0)$ with C_2 eigenvalue ξ , we can construct a state $T_y |0, 0; \xi\rangle$

at $(\pi, 0)$ with the same C_2 eigenvalue:

$$\begin{aligned} C_2 T_y |0, 0; \xi\rangle &= T_y T_y^{-2} C_2 |0, 0; \xi\rangle \\ &= \xi T_y^{-1} |0, 0; \xi\rangle, \end{aligned} \quad (\text{F4})$$

where the first equality is due to the commutation relation Eq. (F1) and the second equality follows because the T_y^2 eigenvalue of a Bloch wave function at k_y is e^{2ik_y} . Similarly, for each Bloch state at $(0, \pi/2)$ with C_2 eigenvalue ξ , there is a state at $(\pi, \pi/2)$ with eigenvalue $-\xi$:

$$\begin{aligned} C_2 T_y |0, \pi/2; \xi\rangle &= T_y T_y^{-2} C_2 |0, \pi/2; \xi\rangle \\ &= \xi T_y T_y^{-2} |0, \pi/2; \xi\rangle \\ &= -\xi T_y |0, \pi/2; \xi\rangle \end{aligned} \quad (\text{F5})$$

It follows that although there are four C_2 symmetric momenta, only two of them have independent eigenvalues, $\Gamma = (0, 0)$ and $Y = (0, \pi/2)$. Each Bloch wave function at those points can have C_2 eigenvalue $+i$ or $-i$.

Due to the unusual behavior of T_y in Eq. (F3), the four momenta invariant under $T_y C_2$ are $(\pm\pi/2, 0)$ and $(\pm\pi/2, \pi/2)$. Similarly only two of them are independent. We choose the two points to be $X = (\pi/2, 0)$ and $M = (\pi/2, \pi/2)$. Since $(T_y C_2)^2 = -1$, there are two irreps for each point and each irrep has $T_y C_2$ eigenvalue $+i, -i$.

We summarize the irreps at all independent high symmetry points for the group $p2$ in Table II. Notice that we have used $C_2^2 = -1$, corresponding to spinful electrons, in the above derivations. If $C_2^2 = +1$, the C_2 eigenvalues will be $+1, -1$.

2. $p4$

We now study the group $p4$ group with $\phi = \pi$ and a 2-by-2 unit cell. The lattice translation group is $\mathbb{T}_M = \{(2n_1, 2n_2) | n_1, n_2 \in \mathbb{Z}\}$. The little co-group is a subgroup of $p4/\mathbb{T}_M$ generated by C_4 and T_x, T_y symmetries.

For the 2-by-2 unit cell, the Brillouin zone is $[-\pi/2, \pi/2] \times [-\pi/2, \pi/2]$. T_x and T_y both map (k_x, k_y) to itself. Since $\{T_x, T_y\} = 0$, each irrep at generic \mathbf{k} is at least two-dimensional.

The two high symmetry points invariant under C_4 are $(0, 0)$ and $(\pi/2, \pi/2)$, while the two high symmetry points invariant under C_2 but not C_4 are $(\pi/2, 0)$ and $(0, \pi/2)$. We study each point separately.

At $X = (\pi/2, 0)$, the (anti-)commutation relations derived from Eqs. (F1) and (F2), $[C_2, T_y] = 0$, $\{C_2, T_x\} = 0$, $\{T_x, T_y\} = 0$ lead to two two-dimensional irreps X_1, X_2 as shown in Table III.

At $Y = (0, \pi/2)$, the (anti-)commutation relations derived from Eqs. (F1) and (F2), $[C_2, T_x] = 0$, $\{C_2, T_y\} = 0$, $\{T_x, T_y\} = 0$ lead to two two-dimensional irreps Y_1, Y_2 as shown in Table III.

At $\Gamma = (0, 0)$, $[C_4 T_x, T_x T_y] = 0$ and $\{T_x T_y, T_x\} = 0$ due to Eqs. (F1) and (F2). For a Bloch eigenstate $|\xi, \eta\rangle$ with eigenvalue $\xi = \pm 1$ or $\pm i$ of $C_4 T_x$ and eigenvalues $\eta = \pm i$ of $T_x T_y$, T_x maps it to an eigenstate of $C_4 T_x$ with

eigenvalue $\eta\xi$ and an eigenstate of $T_x T_y$ with eigenvalue $-\eta$:

$$\begin{aligned} C_4 T_x T_x |\xi, \eta\rangle &= T_y C_4 T_x |\xi, \eta\rangle \\ &= T_x T_x^{-2} T_x T_y C_4 T_x |\xi, \eta\rangle \\ &= T_x e^{-2ik_x} \eta \xi |\xi, \eta\rangle \\ &= \eta \xi T_x |\xi, \eta\rangle \end{aligned} \quad (\text{F6})$$

where the first equality follows Eq. (F1) and

$$\begin{aligned} T_x T_y T_x |\xi, \eta\rangle &= -T_x T_x T_y |\xi, \eta\rangle \\ &= -\eta T_x |\xi, \eta\rangle \end{aligned} \quad (\text{F7})$$

due to Eq. (F2). The two equations pair up eigenvalues and lead to four two-dimensional irreps $\Gamma_1, \Gamma_2, \Gamma_3, \Gamma_4$ as shown in Table III.

At $M = (\pi/2, \pi/2)$, there are (anti-)commutation relations $[C_4, T_x T_y] = 0$ and $\{T_x, T_x T_y\} = 0$. For an eigenstate $|\xi, \eta\rangle$ with eigenvalue $\xi = e^{i\pi/2}, e^{3i\pi/2}, e^{-3i\pi/2}$, or $e^{-i\pi/2}$ of C_4 and eigenvalue $\eta = +i, -i$ of $T_x T_y$, T_x maps it to an eigenstate of C_4 and $T_x T_y$ with eigenvalues $-\eta\xi$ and $-\eta$, respectively:

$$\begin{aligned} C_4 T_x |\xi, \eta\rangle &= T_y C_4 |\xi, \eta\rangle \\ &= T_x T_x^{-2} T_x T_y C_4 |\xi, \eta\rangle \\ &= T_x e^{-2ik_x} \eta \xi |\xi, \eta\rangle \\ &= -\eta \xi T_x |\xi, \eta\rangle \end{aligned} \quad (\text{F8})$$

where the first line comes from Eq. (F1) and

$$\begin{aligned} T_x T_y T_x |\xi, \eta\rangle &= -T_x T_x T_y |\xi, \eta\rangle \\ &= -\eta T_x |\xi, \eta\rangle \end{aligned} \quad (\text{F9})$$

due to Eq. (F2). The commutation relations imply four two-dimensional irreps M_1, M_2, M_3, M_4 as shown in Table III.

3. $p4/m'$

We study the group $p4/m'$ with $\phi = \pi$ and a 2-by-2 unit cell. The lattice translation group and Brillouin zone are the same as for the $p4$ case. We first prove that each band is four-fold degenerate: since $T_x^2 = e^{2ik_x}$, T_x has eigenvalues ηe^{ik_x} , $\eta = \pm 1$. A Bloch eigenstate at k , $|k; \eta\rangle$, is mapped by \mathcal{TI} to another state at k with the same eigenvalue:

$$\begin{aligned} T_x \mathcal{TI} |k; \eta\rangle &= \mathcal{TI} T_x^{-2} T_x |k; \eta\rangle \\ &= \mathcal{TI} \eta e^{-ik_x} |k; \eta\rangle \\ &= \eta e^{ik_x} \mathcal{TI} |k; \eta\rangle \end{aligned} \quad (\text{F10})$$

where the first line can be derived from Table I. In the spinful case where $(\mathcal{TI})^2 = -1$, there is a Kramers degeneracy, i.e. $\mathcal{TI} |k; \eta\rangle$ and $|k; \eta\rangle$ are two different states.

The anticommutation $\{T_x, T_y\} = 0$ implies that T_y flips the eigenstate of T_x :

$$\begin{aligned} T_x T_y |k; \eta\rangle &= -T_y T_x |k; \eta\rangle \\ &= -\eta e^{ik_x} T_y |k; \eta\rangle \end{aligned} \quad (\text{F11})$$

Combining Eqs. (F10) and (F11), we conclude that each eigenstate is at least four-fold degenerate.

We now study the irreps at the high symmetry points Γ, X, Y, M . The role of \mathcal{TI} is to pair the two-dimensional irreps of the $p4$ group. Following the irrep labelling scheme used for $p4$ in the previous section, the irreps are summarized in Table IV and justified as follows:

At $X = (\pi/2, 0)$, the commutation relations $[C_2, \mathcal{TI}] = 0$ and $[T_y, \mathcal{TI}] = 0$ lead to one irrep $X_1 X_2$, and similarly at Y for $Y_1 Y_2$. At $\Gamma = (0, 0)$, the commutation relations $[C_4, \mathcal{TI}] = 0$ leads to one irrep $\Gamma_1 \Gamma_2$. Finally, at $M = (\pi/2, \pi/2)$, the relations $[C_4, \mathcal{TI}] = 0$ and $\{T_x T_y, \mathcal{TI}\} = 0$ lead to three four-dimensional irreps $M_1 M_1, M_3 M_3$, and $M_2 M_4$.

Appendix G: Deriving the symmetry indicator

In this appendix, we describe how to find the symmetry indicator classification of a space group and how to apply it to a group of bands to determine in which topological class the bands belong.

At the crux of the theory is the “EBR matrix” for the space group. Each row of the matrix corresponds to a particular choice of \mathbf{q} and an irrep ρ of $G_{\mathbf{q}}$ (Sec. IV B). Each column corresponds to a particular irrep of the little co-group at a particular high symmetry momentum (Sec. III B). The entry in the matrix indicates the number of times the irrep appears in the band representation ρ_G induced from ρ , as we will define in Eq. (G1) [14, 48, 49].

Let A be an integer EBR matrix of the symmetry group under consideration. Since a group of topologically trivial bands transforms identically to a sum of Wannier functions, its irreps at high symmetry points satisfy

$$v = An, \quad (\text{G1})$$

where v_j is the number of times the j^{th} irrep appears in the band structure [8].

Let the Smith normal form of A be given by

$$A = U^{-1} D V^{-1}, \quad (\text{G2})$$

where D is a diagonal positive integer matrix with diagonal entries $(d_1, \dots, d_M, 0, \dots, 0)$, i.e., the first M entries are positive and the remaining entries are zero, and U, V are integer matrices invertible over the integers. The stable topological classification for the space group is given by

$$\mathbb{Z}_{d_1} \times \dots \times \mathbb{Z}_{d_M}. \quad (\text{G3})$$

The Smith normal form matrices are

$$D = \begin{pmatrix} 1 & 0 & 0 & 0 & 0 & 0 & 0 & 0 & 0 & 0 \\ 0 & 1 & 0 & 0 & 0 & 0 & 0 & 0 & 0 & 0 \\ 0 & 0 & 1 & 0 & 0 & 0 & 0 & 0 & 0 & 0 \\ 0 & 0 & 0 & 1 & 0 & 0 & 0 & 0 & 0 & 0 \\ 0 & 0 & 0 & 0 & 1 & 0 & 0 & 0 & 0 & 0 \\ 0 & 0 & 0 & 0 & 0 & 1 & 0 & 0 & 0 & 0 \\ 0 & 0 & 0 & 0 & 0 & 0 & 1 & 0 & 0 & 0 \\ 0 & 0 & 0 & 0 & 0 & 0 & 0 & 1 & 0 & 0 \\ 0 & 0 & 0 & 0 & 0 & 0 & 0 & 0 & 8 & 0 \\ 0 & 0 & 0 & 0 & 0 & 0 & 0 & 0 & 0 & 0 \end{pmatrix} \quad (\text{G20})$$

$$U = \begin{pmatrix} 0 & -1 & -1 & 0 & 1 & 1 & 0 & 1 & 0 & 0 \\ -1 & -1 & -1 & 0 & 1 & 1 & 1 & 1 & 0 & 0 \\ 0 & -1 & -1 & 0 & 1 & 1 & 1 & 2 & -1 & 0 \\ -1 & -1 & -1 & 0 & 2 & 1 & 1 & 2 & -1 & 0 \\ 0 & 1 & 1 & 0 & 0 & -1 & 0 & -1 & 0 & 0 \\ 0 & 1 & 1 & 0 & -1 & -1 & -1 & -1 & 1 & 0 \\ -1 & 0 & 1 & 0 & 0 & -1 & 0 & -1 & 1 & 0 \\ 6 & 4 & 2 & 0 & -9 & -3 & -5 & -7 & 4 & 0 \\ 1 & 1 & 1 & 1 & -1 & -1 & -1 & -1 & 0 & 0 \\ 0 & 0 & 0 & 0 & -1 & -1 & -1 & -1 & 1 & 1 \end{pmatrix} \quad (\text{G21})$$

$$V = \begin{pmatrix} 1 & 0 & 0 & -3 & 0 & 0 & -1 & -5 & -1 & -1 \\ 0 & 1 & 0 & -2 & 0 & 0 & -1 & -3 & -1 & -1 \\ 0 & 0 & 1 & -1 & 0 & 0 & 0 & -1 & -1 & -1 \\ 0 & 0 & 0 & 1 & 0 & 0 & 0 & 1 & -1 & -1 \\ 0 & 0 & 0 & 1 & 1 & 0 & 0 & 2 & 1 & 0 \\ 0 & 0 & 0 & -2 & 0 & 1 & -1 & -4 & 1 & 0 \\ 0 & 0 & 0 & -1 & 0 & 0 & 0 & -2 & 1 & 0 \\ 0 & 0 & 0 & 0 & 0 & 0 & 0 & 0 & 1 & 0 \\ 0 & 0 & 0 & 2 & 0 & 0 & 1 & 4 & 0 & 1 \\ 0 & 0 & 0 & 0 & 0 & 0 & 0 & 0 & 0 & 1 \end{pmatrix} \quad (\text{G22})$$

The stable indicators is given by Eq. (44) in the main text,

$$\begin{aligned} \text{index} = & 2\#\Gamma_1 + 4\#\Gamma_2 - 2\#\Gamma_3 + \#M_1 + 3\#M_2 \\ & - 3\#M_3 - \#M_4 + 4\#X_1 \pmod{8}, \end{aligned} \quad (\text{G23})$$

which corresponds to the 8 in the diagonal of D .

The symmetry indicators for Wannier centers are

$$e_{4a} = 2(2\#\Gamma_2 + 2\#\Gamma_3 + \#M_2 + \#M_4 + 2\#X_2) \pmod{8} \quad (\text{G24})$$

$$e_{4b} = 2(2\#\Gamma_2 + 2\#\Gamma_3 - \#M_2 - \#M_4 - N/2) \pmod{8} \quad (\text{G25})$$

$$e_{8c} = \#X_1 - \#X_2 \pmod{4} \quad (\text{G26})$$

3. $p4/m'$

The basis for band representations (columns) and the basis for coefficients of EBRs (rows) are

$$(\Gamma_1\Gamma_4, \Gamma_2\Gamma_3, M_1M_1, M_3M_3, M_2M_4), \quad (\text{G27})$$

where Π_i is defined in Table IV, and

$$(\bar{E}_{1/2}^{4a}, \bar{E}_{3/2}^{4a}, {}^1\bar{E}_{1/2}^{4b}, {}^2\bar{E}_{3/2}^{4b}, {}^1\bar{E}_{3/2}^{4b}, {}^1\bar{E}_{3/2}^{4b}, {}^2\bar{E}_{1/2}^{4b}, {}^2\bar{E}_{1/2}^{4b}, \bar{E}^{8c}). \quad (\text{G28})$$

where \bar{E}^{nw} is an irrep of the site symmetry group of the Wyckoff position labelled by nw . \bar{E}_{jz}^{4a} has C_4 eigenvalues $e^{\pm i\frac{\pi}{2}jz}$, while ${}^1\bar{E}_{jz}^{4b}$ and ${}^2\bar{E}_{jz}^{4b}$ correspond to eigenvalues $e^{i\frac{\pi}{2}jz}$ and $e^{-i\frac{\pi}{2}jz}$ of $C_4(\frac{1}{2}, \frac{1}{2})$ separately. For the site-symmetry group of the $4a$ position, there are two irreps $\bar{E}_{1/2}^{4a}$ and $\bar{E}_{3/2}^{4a}$, while for the site-symmetry group of the $4b$ position, there are three irreps, ${}^1\bar{E}_{1/2}^{4b}$, ${}^2\bar{E}_{1/2}^{4b}$, ${}^1\bar{E}_{3/2}^{4b}$ and ${}^2\bar{E}_{3/2}^{4b}$. The difference between these comes from the unusual pairing of irreps with $C_4(\frac{1}{2}, \frac{1}{2})$ eigenvalues ξ and $-i\xi^*$ as derived in Eq. (21). For the site-symmetry group of the $8c$ position, there is only one irrep, \bar{E}^{8c} , with $C_2(\frac{1}{2}, 0)$ eigenvalues $\pm i$.

In this basis, the EBR matrix is

$$A = \begin{pmatrix} 1 & 1 & 1 & 2 & 2 \\ 1 & 1 & 1 & 0 & 2 \\ 1 & 0 & 0 & 1 & 1 \\ 0 & 1 & 0 & 1 & 1 \\ 1 & 1 & 2 & 0 & 2 \end{pmatrix} \quad (\text{G29})$$

The Smith normal form matrices are

$$D = \begin{pmatrix} 1 & 0 & 0 & 0 & 0 \\ 0 & 1 & 0 & 0 & 0 \\ 0 & 0 & 1 & 0 & 0 \\ 0 & 0 & 0 & 2 & 0 \\ 0 & 0 & 0 & 0 & 0 \end{pmatrix} \quad (\text{G30})$$

$$U = \begin{pmatrix} 0 & 0 & 1 & 0 & 0 \\ 0 & 0 & 0 & 1 & 0 \\ 1 & 0 & -1 & -1 & 0 \\ 1 & -1 & 0 & 0 & 0 \\ -1 & -1 & 1 & 1 & 1 \end{pmatrix} \quad (\text{G31})$$

$$V = \begin{pmatrix} 1 & 0 & 0 & -1 & -1 \\ 0 & 1 & 0 & -1 & -1 \\ 0 & 0 & 1 & 0 & 0 \\ 0 & 0 & 0 & 1 & 0 \\ 0 & 0 & 0 & 0 & 1 \end{pmatrix} \quad (\text{G32})$$

The stable indicator is given by Eq. (48) in the main text,

$$\text{index}_1 = N/4 \pmod{2}. \quad (\text{G33})$$

The symmetry indicators for Wannier centers are

$$e_{4a} = \frac{N}{2} + 2(\#M_1M_1 + \#M_3M_3) \pmod{4} \quad (\text{G34})$$

$$e_{4b} = -\frac{N}{4} + 2(\#M_1M_1 + \#M_3M_3) \pmod{4} \quad (\text{G35})$$

$$e_{8c} = 0 \pmod{2} \quad (\text{G36})$$

	$\Gamma(0,0)$					
Irrep	Γ_1	Γ_2	Γ_3	Γ_4	Γ_5	Γ_6
ξ	1	$e^{i\pi/3}$	$e^{i2\pi/3}$	-1	$-e^{i\pi/3}$	$-e^{i2\pi/3}$

TABLE VIII. An irrep at Γ is labeled with ξ which has C_6 eigenvalues $\epsilon\xi$ and $\bar{\epsilon}\xi$, where $\epsilon = e^{i2\pi/3}$.

	$K(1/3, 2/3)$		
Irrep	K_1	K_2	K_3
ξ	1	$e^{i2\pi/3}$	$e^{-i2\pi/3}$

TABLE IX. An irrep at K is labeled with ξ which corresponds to C_3 eigenvalues $\epsilon\xi$ and $\bar{\epsilon}\xi$, where $\epsilon = e^{i2\pi/3}$.

	$M(1/2, 0)$	
Irrep	M_1	M_2
C_2	σ_z	$-\sigma_z$
$T(\hat{\mathbf{a}}_2)$	σ_z	σ_z

TABLE X. The irreps of M are given in the basis such that $T(\hat{\mathbf{a}}_1) = i\sigma_y$ and $T(\hat{\mathbf{a}}_2) = \sigma_z$.

	$\Gamma(0,0)$			
Irrep	Γ_1	Γ_2	Γ_3	Γ_4
$C_4T(\hat{\mathbf{x}})$	$\begin{pmatrix} 1 & \\ & i \end{pmatrix} \epsilon$	$\begin{pmatrix} i & \\ & -1 \end{pmatrix} \epsilon$	$\begin{pmatrix} -1 & \\ & -i \end{pmatrix} \epsilon$	$\begin{pmatrix} -i & \\ & 1 \end{pmatrix} \epsilon$
$T(\hat{\mathbf{x}})T(\hat{\mathbf{y}})$	$i\sigma_z$	$i\sigma_z$	$i\sigma_z$	$i\sigma_z$

	$M(\pi/2, \pi/2)$			
Irrep	M_1	M_2	M_3	M_4
C_4	$\begin{pmatrix} 1 & \\ & i \end{pmatrix}$	$\begin{pmatrix} i & \\ & -1 \end{pmatrix}$	$\begin{pmatrix} -1 & \\ & -i \end{pmatrix}$	$\begin{pmatrix} -i & \\ & 1 \end{pmatrix}$
$T(\hat{\mathbf{x}})T(\hat{\mathbf{y}})$	$i\sigma_z$	$i\sigma_z$	$i\sigma_z$	$i\sigma_z$

	$X(1/2, 0)$	
Irrep	X_1	X_2
C_2	σ_z	$-\sigma_z$
$T(\hat{\mathbf{y}})$	σ_z	σ_z

TABLE XI. High symmetry momenta (first row) and the irreps (second row) of their little co-group for the group $p4$. Subsequent rows list the eigenvalue of the indicated symmetry with $\epsilon = e^{i\pi/4}$.

Appendix H: Chern number indicators with n -fold rotation symmetry at π -flux and no spin-orbit coupling

In this section we use our theory to derive the Chern number symmetry indicators for C_4 , C_6 and C_3 rotational symmetric systems in $\phi = \pi$ flux. We consider the case without time-reversal symmetry or spin-orbit coupling.

1. Irreps of the little co-groups

Consider a two dimensional lattice system with C_n rotation symmetry. We choose the q -by- q unit cell for $2\pi p/q$ magnetic flux. The little co-group at a high-

symmetry momentum point k is $\tilde{G}_k = C_n \ltimes \mathbb{T}_k$, where $\mathbb{T}_k = \mathbb{T}/\mathbb{T}_M$. \mathbb{T} is generated by $T(\hat{\mathbf{a}}_1), T(\hat{\mathbf{a}}_2)$ and \mathbb{T}_M is generated by $T(q\hat{\mathbf{a}}_1), T(q\hat{\mathbf{a}}_2)$; thus, $|\mathbb{T}_k| = q^2$. The rotation group has n elements, $|C_n| = n$. Therefore, according to Eq. (33), at $2\pi p/q$ flux there are n distinct q -dimensional projective irreps.

At π flux, we choose a basis such that the translations are represented by

$$T(\hat{\mathbf{a}}_1) = e^{ik_1} \sigma_x, \quad (\text{H1})$$

$$T(\hat{\mathbf{a}}_2) = e^{ik_2} \sigma_y, \quad (\text{H2})$$

$$T(\hat{\mathbf{a}}_3) = -e^{i(k_2 - k_1)} \sigma_z, \quad (\text{H3})$$

where $\hat{\mathbf{a}}_3 = \hat{\mathbf{a}}_2 - \hat{\mathbf{a}}_1$. For the four-fold symmetric case ($n = 4$), the lattice vectors are $q\mathbf{a}_1 = q(1, 0)$, $q\mathbf{a}_2 = q(0, 1)$, and the reciprocal lattice vectors are $\mathbf{b}_1/q = (1, 0)/q$, $\mathbf{b}_2/q = (0, 1)/q$ in Cartesian coordinates; for the three- and six-fold symmetric cases ($n = 3, 6$), the lattice vectors are $q\mathbf{a}_1 = q(1, 0)$, $q\mathbf{a}_2 = q(\frac{1}{2}, \frac{\sqrt{3}}{2})$, and the reciprocal lattice vectors are $\mathbf{b}_1/q = (1, -1/\sqrt{3})/q$, $\mathbf{b}_2/q = (0, 2/\sqrt{3})/q$ in Cartesian coordinates.

In this basis, the representation matrix for C_n is obtained by solving the equation

$$C_n T(\mathbf{a}) = T(R_n \mathbf{a}) C_n \quad (\text{H4})$$

for any C_n -invariant momentum point. We further require the C_n matrices to satisfy $C_n^n = 1$. Then there are n solutions corresponding to the n overall phases ξ , each of which is a distinct irreducible representation of \tilde{G}_k . From this equation, we find the C_6 , C_3 and C_4 matrices explicitly:

- The C_6 symmetry operator at $\Gamma = (0, 0)$ is

$$C_6 = -\frac{1}{2} (\sigma_0 + i(\sigma_x + \sigma_y + \sigma_z)) \xi \quad (\text{H5})$$

where $\xi = e^{i(j-1)\pi/3}$, $j = 1, \dots, 6$ labels the irrep.

- The C_3 operator at Γ and K is the square of this C_6 matrix.
- The C_4 symmetry operator at $\Gamma = (0, 0)$ is $(\sigma_x + \sigma_y)\xi/\sqrt{2}$, while the C_4 symmetry operator at $M = (1/2, 1/2)$ is $(\sigma_0 - i\sigma_z)\xi/\sqrt{2}$, where $\xi = 1, i, -1, -i$.

The irreps obtained by this method for the point group $p6$ are listed in Tables VIII, IX and X for Γ , K , and M , respectively. The irreps for the point group $p3$ at $\Gamma = (0, 0)$, $K = (1/3, 2/3)$, $K' = (2/3, 1/3)$ are all isomorphic to the irreps of K in $p6$ shown in Table IX. The irreps for the point group $p4$ are listed in Table XI. The irreps are isomorphic to those that appear for the spinful case in Table III which could also be derived using Eq. (H4).

The discussion above pertains to irreps of the little co-group of a point in momentum space. We now derive the irreps of the site symmetry group of each Wyckoff position in real space. While the site symmetry groups

are the same as for the non-magnetic cases, and therefore, the irreps remain the same, the elementary band representations induced from these irreps are fundamentally different from the non-magnetic cases. We compute these induced representations using Eq. (41) for $p4$, $p6$ and $p3$. The resulting EBR matrices are shown in the following.

2. Chern number indicators

a. $p4$

For wallpaper group $p4$, all the irreps in the spinless cases are isomorphic to the spinful cases. Therefore, the EBR matrix and the symmetry indicators are the same as the spinful case shown in Appendix G. We conclude that the indicator is

$$\text{index} = 2\#\Gamma_1 + 4\#\Gamma_2 - 2\#\Gamma_3 + \#M_1 + 3\#M_2 - 3\#M_3 - \#M_4 + 4\#X_1 \pmod{8}, \quad (\text{H6})$$

where the irreps Π_j are defined in Table XI.

b. $p6$

The basis for band representations (columns) and the basis for coefficients of EBRs (rows) are

$$(\Gamma_1, \Gamma_2, \Gamma_3, \Gamma_4, \Gamma_5, \Gamma_6, K_1, K_2, K_3, M_1, M_2), \quad (\text{H7})$$

where Π_i is defined in Tables VIII, IX and X, and

$$(\Gamma_1^{4a}, \Gamma_2^{4a}, \Gamma_3^{4a}, \Gamma_4^{4a}, \Gamma_5^{4a}, \Gamma_6^{4a}, \Gamma_1^{8b}, \Gamma_2^{8b}, \Gamma_3^{8b}, \Gamma_1^{12c}, \Gamma_2^{12c}), \quad (\text{H8})$$

where Γ_j^{nw} is an irrep of the site symmetry group of the Wyckoff position labelled by nw . Γ_j^{4a} has C_6 eigenvalue $e^{i(j-1)\pi/3}$, $j = 1, \dots, 6$, Γ_j^{8b} has C_3 eigenvalue $e^{i(j-1)2\pi/3}$, $j = 1, 2, 3$, and Γ_j^{12c} has C_2 eigenvalue $+1, -1$. In this basis, the EBR matrix is

$$A = \begin{pmatrix} 0 & 0 & 1 & 0 & 1 & 0 & 1 & 1 & 0 & 1 & 1 \\ 0 & 0 & 0 & 1 & 0 & 1 & 0 & 1 & 1 & 1 & 1 \\ 1 & 0 & 0 & 0 & 1 & 0 & 1 & 0 & 1 & 1 & 1 \\ 0 & 1 & 0 & 0 & 0 & 1 & 1 & 1 & 0 & 1 & 1 \\ 1 & 0 & 1 & 0 & 0 & 0 & 0 & 1 & 1 & 1 & 1 \\ 0 & 1 & 0 & 1 & 0 & 0 & 1 & 0 & 1 & 1 & 1 \\ 0 & 1 & 1 & 0 & 1 & 1 & 1 & 1 & 2 & 2 & 2 \\ 1 & 0 & 1 & 1 & 0 & 1 & 2 & 1 & 1 & 2 & 2 \\ 1 & 1 & 0 & 1 & 1 & 0 & 1 & 2 & 1 & 2 & 2 \\ 1 & 1 & 1 & 1 & 1 & 1 & 2 & 2 & 2 & 4 & 2 \\ 1 & 1 & 1 & 1 & 1 & 1 & 2 & 2 & 2 & 2 & 4 \end{pmatrix} \quad (\text{H9})$$

The Smith normal form matrices are

$$D = \begin{pmatrix} 1 & 0 & 0 & 0 & 0 & 0 & 0 & 0 & 0 & 0 & 0 \\ 0 & 1 & 0 & 0 & 0 & 0 & 0 & 0 & 0 & 0 & 0 \\ 0 & 0 & 1 & 0 & 0 & 0 & 0 & 0 & 0 & 0 & 0 \\ 0 & 0 & 0 & 1 & 0 & 0 & 0 & 0 & 0 & 0 & 0 \\ 0 & 0 & 0 & 0 & 1 & 0 & 0 & 0 & 0 & 0 & 0 \\ 0 & 0 & 0 & 0 & 0 & 1 & 0 & 0 & 0 & 0 & 0 \\ 0 & 0 & 0 & 0 & 0 & 0 & 1 & 0 & 0 & 0 & 0 \\ 0 & 0 & 0 & 0 & 0 & 0 & 0 & 1 & 0 & 0 & 0 \\ 0 & 0 & 0 & 0 & 0 & 0 & 0 & 0 & 12 & 0 & 0 \\ 0 & 0 & 0 & 0 & 0 & 0 & 0 & 0 & 0 & 0 & 0 \\ 0 & 0 & 0 & 0 & 0 & 0 & 0 & 0 & 0 & 0 & 0 \end{pmatrix} \quad (\text{H10})$$

$$U = \begin{pmatrix} -1 & 0 & 0 & 0 & 0 & -1 & 1 & 1 & 1 & -1 & 0 \\ -1 & 0 & 0 & 0 & 0 & 0 & 1 & 0 & 0 & 0 & 0 \\ 0 & 0 & -1 & 0 & 0 & -1 & 1 & 1 & 1 & -1 & 0 \\ -1 & 0 & -1 & -1 & -1 & -1 & 1 & 1 & 1 & 0 & 0 \\ -1 & 0 & 0 & -1 & -1 & -1 & 2 & 1 & 1 & -1 & 0 \\ -1 & 0 & -1 & 0 & -1 & -2 & 1 & 1 & 1 & 0 & 0 \\ 1 & 0 & 0 & 1 & 0 & 0 & -1 & 0 & 0 & 0 & 0 \\ 1 & 0 & 3 & -1 & 2 & 5 & -2 & -3 & -4 & 2 & 0 \\ 2 & 0 & 10 & -4 & 6 & 16 & -5 & -9 & -13 & 6 & 0 \\ 1 & 1 & 1 & 1 & 1 & 1 & -1 & -1 & -1 & 0 & 0 \\ 0 & 0 & 0 & 0 & 0 & 0 & -1 & -1 & -1 & 1 & 1 \end{pmatrix} \quad (\text{H11})$$

$$V = \begin{pmatrix} 1 & 0 & 0 & 0 & 0 & 0 & -1 & 5 & -1 & -1 \\ 0 & 1 & 0 & 0 & 0 & -1 & 0 & -2 & 7 & -1 & -1 \\ 0 & 0 & 1 & 0 & 0 & 0 & -2 & 9 & -1 & -1 \\ 0 & 0 & 0 & 1 & 0 & -1 & 0 & -3 & 11 & -1 & -1 \\ 0 & 0 & 0 & 0 & 1 & 0 & 0 & 0 & 1 & -1 & -1 \\ 0 & 0 & 0 & 0 & 0 & 0 & -4 & 15 & -1 & -1 \\ 0 & 0 & 0 & 0 & 0 & 0 & 1 & 0 & 0 & 1 & 0 \\ 0 & 0 & 0 & 0 & 0 & 0 & 2 & -8 & 1 & 0 & 0 \\ 0 & 0 & 0 & 0 & 0 & 0 & 1 & -4 & 1 & 0 & 0 \\ 0 & 0 & 0 & 0 & 0 & 1 & 0 & 3 & -10 & 0 & 1 \\ 0 & 0 & 0 & 0 & 0 & 0 & 1 & -4 & 0 & 1 & 1 \end{pmatrix} \quad (\text{H12})$$

The stable indicator is

$$\text{index} = 2\#\Gamma_1 - 2\#\Gamma_3 - 4\#\Gamma_4 + 6\#\Gamma_5 + 4\#\Gamma_6 - 5\#K_1 + 3\#K_2 - \#K_3 + 6\#M_1 \pmod{12}, \quad (\text{H13})$$

where the modulus corresponds to the 12 in the diagonal of D .

c. $p3$

The basis for band representations (columns) and the basis for coefficients of EBRs (rows) are

$$(\Gamma_1, \Gamma_2, \Gamma_3, K_1, K_2, K_3, K'_1, K'_2, K'_3), \quad (\text{H14})$$

where Π_i is defined in Table IX and

$$(\Gamma_1^{4a}, \Gamma_2^{4a}, \Gamma_3^{4a}, \Gamma_1^{4b}, \Gamma_2^{4b}, \Gamma_3^{4b}, \Gamma_1^{4c}, \Gamma_2^{4c}, \Gamma_3^{4c}), \quad (\text{H15})$$

where Γ_j^{nw} is an irrep of the site symmetry group of the Wyckoff position labelled by nw . Γ_j^{nw} has C_3 eigenvalue $e^{i(j-1)2\pi/3}$, $j = 1, 2, 3$. In this basis, the EBR matrix is

$$A = \begin{pmatrix} 0 & 1 & 1 & 1 & 1 & 0 & 1 & 1 & 0 \\ 1 & 0 & 1 & 0 & 1 & 1 & 0 & 1 & 1 \\ 1 & 1 & 0 & 1 & 0 & 1 & 1 & 0 & 1 \\ 0 & 1 & 1 & 1 & 0 & 1 & 0 & 1 & 1 \\ 1 & 0 & 1 & 1 & 1 & 0 & 1 & 0 & 1 \\ 1 & 1 & 0 & 0 & 1 & 1 & 1 & 1 & 0 \\ 0 & 1 & 1 & 0 & 1 & 1 & 1 & 0 & 1 \\ 1 & 0 & 1 & 1 & 0 & 1 & 1 & 1 & 0 \\ 1 & 1 & 0 & 1 & 1 & 0 & 0 & 1 & 1 \end{pmatrix} \quad (\text{H16})$$

The Smith normal form matrices are

$$D = \begin{pmatrix} 1 & 0 & 0 & 0 & 0 & 0 & 0 & 0 & 0 \\ 0 & 1 & 0 & 0 & 0 & 0 & 0 & 0 & 0 \\ 0 & 0 & 1 & 0 & 0 & 0 & 0 & 0 & 0 \\ 0 & 0 & 0 & 1 & 0 & 0 & 0 & 0 & 0 \\ 0 & 0 & 0 & 0 & 1 & 0 & 0 & 0 & 0 \\ 0 & 0 & 0 & 0 & 0 & 1 & 0 & 0 & 0 \\ 0 & 0 & 0 & 0 & 0 & 0 & 6 & 0 & 0 \\ 0 & 0 & 0 & 0 & 0 & 0 & 0 & 0 & 0 \\ 0 & 0 & 0 & 0 & 0 & 0 & 0 & 0 & 0 \end{pmatrix} \quad (\text{H17})$$

$$U = \begin{pmatrix} 0 & 1 & 0 & 0 & -1 & 0 & 0 & 1 & 0 \\ -1 & 0 & 0 & 1 & 0 & 0 & 1 & 0 & 0 \\ 0 & 1 & 0 & 0 & -1 & -1 & 1 & 1 & 0 \\ 1 & 0 & 0 & 0 & 0 & 0 & -1 & 0 & 0 \\ 2 & 1 & 0 & -1 & -1 & 0 & -1 & 0 & 0 \\ 1 & 0 & 0 & -1 & -1 & 0 & 0 & 1 & 0 \\ 2 & -2 & 0 & -1 & 1 & 3 & -4 & -2 & 0 \\ 1 & 1 & 1 & -1 & -1 & -1 & 0 & 0 & 0 \\ 0 & 0 & 0 & -1 & -1 & -1 & 1 & 1 & 1 \end{pmatrix} \quad (\text{H18})$$

$$V = \begin{pmatrix} 1 & 0 & -2 & 0 & 0 & 0 & -3 & -1 & -1 \\ 0 & 1 & 0 & 0 & 0 & 0 & 1 & -1 & -1 \\ 0 & 0 & 0 & 0 & 0 & 0 & -1 & -1 & -1 \\ 0 & 0 & -1 & 1 & 0 & 0 & -2 & 1 & 0 \\ 0 & 0 & -2 & 0 & 1 & 0 & -4 & 1 & 0 \\ 0 & 0 & 0 & 0 & 0 & 0 & 0 & 1 & 0 \\ 0 & 0 & -1 & 0 & 0 & 1 & -2 & 0 & 1 \\ 0 & 0 & 1 & 0 & 0 & 0 & 2 & 0 & 1 \\ 0 & 0 & 0 & 0 & 0 & 0 & 0 & 0 & 1 \end{pmatrix} \quad (\text{H19})$$

The stable indicator is

$$\text{index} = 2\#\Gamma_1 - 2\#\Gamma_2 - \#K_1 + \#K_2 + 3\#K_3 + 2\#K'_1 - 2\#K'_2 \pmod{6}, \quad (\text{H20})$$

where the modulus corresponds to the 6 in the diagonal of D .

Appendix I: Symmetry indicator for the Chern number

The Chern number in a four-fold symmetric system is given by Eq. (45) [22]:

$$e^{i\frac{\pi}{2}C} = (-)^{2SN} w_{C_4}^\Gamma w_{C_2}^X w_{C_4}^M, \quad (\text{I1})$$

where $S = 1/2$ for spinful systems and w_g^Π is the product of eigenvalues of the symmetry g for filled bands at momentum Π . We now rewrite this formula in terms of the irreps of the little co-groups for $p4$.

From the irreps of $p4$ listed in Table III, it is evident that $w_{C_2}^X \equiv +1$ for both irreps X_1 and X_2 . For the four irreps at M , $w_{C_4}^{M_1} = w_{C_4}^{M_3} = +1$ and $w_{C_4}^{M_2} = w_{C_4}^{M_4} = -1$, where the superscript is now labeling the irrep.

We now find the C_4 eigenvalues of irreps at Γ . We know from Appendix F that for an eigenstate $|\xi, \eta\rangle$ with an eigenvalue ξ of $C_4 T_x$, and η of $T_x T_y$, there is a degenerate state $T_x |\xi, \eta\rangle$ with eigenvalues:

$$C_4 T_x T_x |\xi, \eta\rangle = \xi \eta T_x |\xi, \eta\rangle \quad (\text{I2})$$

$$T_x T_y T_x |\xi, \eta\rangle = -\eta T_x |\xi, \eta\rangle \quad (\text{I3})$$

Neither of these states is separately an eigenstate of C_4 , but we can find a linear combination that is an eigenstate by solving the eigenvalue equation

$$C_4 (\alpha |\xi, \eta\rangle + \beta T_x |\xi, \eta\rangle) = \lambda (\alpha |\xi, \eta\rangle + \beta T_x |\xi, \eta\rangle) \quad (\text{I4})$$

Using the equations above and $T_x^2 = 1$, one finds $\lambda = \pm \sqrt{\xi^2 \eta}$. Therefore, for the four irreps at Γ listed in Table III, $w_{C_4}^{\Gamma_1} = w_{C_4}^{\Gamma_3} = +i$ and $w_{C_4}^{\Gamma_2} = w_{C_4}^{\Gamma_4} = -i$.

Plug these $w_{C_n}^{\Pi_i}$ of irreps into Eq. (II), we get Eq. (46)

$$C = 2N + \#\Gamma_1 + \#\Gamma_3 - \#\Gamma_2 - \#\Gamma_4 + 2(\#M_2 + \#M_4) \pmod{4}. \quad (\text{I5})$$

Appendix J: Symmetry analysis at other fluxes

In this section, we apply the non-magnetic symmetry indicators (i.e. ignoring the sublattice symmetries) to analyze fluxes $\phi/2\pi = 0, 1/5, 2/5$. The Wyckoff positions are defined in Fig. 6(b).

For $\phi = 0$, the layer group is $p4/m'mm$. The symmetry indicators of Wannier centers are [31]

$$e_{1a'} = N - 2[M_{\frac{1}{2}}] \pmod{4} \quad (\text{J1})$$

$$e_{1b'} = 2[M_{\frac{1}{2}}] \pmod{4} \quad (\text{J2})$$

where N is the number of filled bands and $[M_{\frac{1}{2}}] = \#M_{\frac{1}{2}} - \#\Gamma_{\frac{1}{2}}$, where $\#\Pi_{\frac{1}{2}}$ indicates the number of times the two-dimensional irrep $E_{\frac{1}{2}}$ (C_4 eigenvalues $e^{i\pi/4}$, $e^{-i\pi/4}$) appears in the valence bands at the high-symmetry point $\Pi = \Gamma, M$.

For $\phi = \frac{2\pi}{5}, \frac{4\pi}{5}$, the layer group is $p4$. The symmetry indicators are [31]

$$e_{1a'} = N - [X_2] + \frac{3}{2}([M_1] + [M_3]) + 2[M_2] \pmod{4} \quad (\text{J3})$$

$$e_{1b'} = [X_2] - \frac{1}{2}([M_1] + [M_3]) - 2[M_2] \pmod{4} \quad (\text{J4})$$

$$e_{2c'} = -\frac{1}{2}([M_1] + [M_3]) \pmod{2} \quad (\text{J5})$$

$\phi/2\pi$	$\#\Gamma_{\frac{1}{2}}$	$\#M_{\frac{1}{2}}$	N	$e_{1a'} \bmod 4$	$e_{1b'} \bmod 4$	$a_{1a'} \bmod 4$	$\eta \bmod 4$	Phase
0	0	1	2	0	2	2	2	OAL
1/2	2	3	8	2	2	2	0	Trivial

TABLE XII. Evaluation of symmetry indicators in Eqs. (J1) and (J2) at half filling of the OAL model at $\phi = 0$ (middle row) and $\phi = \pi$ (last row).

$\phi/2\pi$	$[X_2]$	$[M_1 + M_3]$	$[M_2]$	N	$e_{1a'} \bmod 4$	$e_{1b'} \bmod 4$	$e_{2c'} \bmod 2$	$a_{1a'} \bmod 4$	$\eta \bmod 4$	Phase
1/5	0	0	1	50	0	2	0	2	2	OAL
2/5	0	0	0	50	2	0	0	2	0	Trivial

TABLE XIII. Evaluation of symmetry indicators Eqs. (J3), (J4), and (J5) at half filling of the OAL model at $\phi = 2\pi/5$ (middle row) and $\phi = 4\pi/5$ (last row).

Here we use the notation $[M_j] = \#M_j - \#\Gamma_j$, where $j = 1, 2, 3, 4$ corresponds to the irrep with C_4 eigenvalue $\exp(i\frac{\pi}{2}(j - \frac{1}{2}))$, and $[X_1] = \#X_1 - \#\Gamma_1 - \#\Gamma_3$, $[X_2] = \#X_2 - \#\Gamma_2 - \#\Gamma_4$, where $X_{1,2}$ corresponds to the irrep with C_2 eigenvalues $+i, -i$. $\#\Pi_j$ indicates the number of times the irrep Π_j appears in the valence bands at the high-symmetry point Π .

The OAL phase and corner charges are indicated by the filling anomaly η . The filling anomaly is defined as the electron number difference between neutral and symmetric configurations for a symmetric finite system [20]. In the absence of polarization, nonzero η implies that the ion charge at $1a'$ Wyckoff position is not equal to the electron charge corresponding to the Wannier functions centered at $1a'$ [31, 51]

$$\begin{aligned} \eta &= N_{e,\text{neutral}} - N_{e,\text{symmetric}} \bmod 4 \\ &= a_{1a'} - e_{1a'} \bmod 4 \end{aligned} \quad (\text{J6})$$

where $a_{1a'}$ and $e_{1a'}$ are the ion charge and electron charge in units of $|e|$ at $1a'$ position. The modulus 4 is specific for our model. In the absence of polarization, the corner charge is given by $Q_c = \eta/4 \bmod 1$.

The non-magnetic symmetry indicators of the model described in Sec. V at 0 and π -flux are shown in Table XII. The indicators at $2\pi/5$ and $4\pi/5$ -flux are in Table XIII. The symmetry indicators show that the system at 0 and $2\pi/5$ -flux is an OAL and at $4\pi/5$ and π flux is trivial. These results are consistent agree with the open-boundary Hofstadter spectrum in Fig. 5.

The filling anomaly cannot jump when C_4 symmetry is preserved, unless the bulk gap or the surface gap closes. In this model, the bulk gap closes between 0 and π flux, as shown in Fig. 5. The gap closing corresponds to the transition between two distinct atomic insulating phases that have different Wannier centers.

Appendix K: Wilson loop and nested Wilson loop

An alternative topological invariant that characterizes the model in Sec. V is the quadrupole moment Q_{xy} , or equivalently the Wilson loop of Wilson loop (nested Wilson loop) [19].

For discrete tight binding models, the Wilson loop is defined as [19, 52, 53]

$$[W_C(\mathbf{k}_0)]_{mn} = \langle u_m(\mathbf{k}_0) | \prod_{\mathbf{k} \in C} \mathcal{P}(\mathbf{k}) | u_n(\mathbf{k}_0) \rangle \quad (\text{K1})$$

where $\mathcal{P}(\mathbf{k}) = \sum_{l=1}^{n_{occ}} |u_l(\mathbf{k})\rangle \langle u_l(\mathbf{k})|$ is the projector onto occupied bands, C is a loop in the Brillouin zone and \mathbf{k}_0 is the base point. We consider two Wilson loops: $W_x(k_x^0, k_y)$ with the path $k_x : 0 \rightarrow 2\pi$ and $W_y(k_x, k_y^0)$ with the path $k_y : 0 \rightarrow 2\pi$. The Wilson loop matrices are not gauge invariant since they depend on the gauge choice of Bloch wavefunctions. However, the eigenvalues of the Wilson loop matrices are gauge invariant. Since Wilson loops are unitary, their eigenvalues are unit complex number of the form $e^{2\pi i \nu}$. We plot $\nu_x(k_y)$ for $W_x(k_y)$ and $\nu_y(k_x)$ for $W_y(k_x)$ for the half filling gap for several fluxes in Fig. 7. The eigenvalue $\nu_x(k_y)$ has a physical meaning, namely the x -coordinate of the hybrid Wannier function $|w(x, k_y)\rangle$. The polarization is determined by the trace of the Wilson loop matrix ν [20, 54]

$$p_x = \int \frac{k_y}{2\pi} \frac{1}{2\pi} \text{Im} (\text{tr} \log W_x(k_y)), \quad (\text{K2})$$

which is equal to the sum of Wilson loop eigenvalues. In our model, polarization vanishes at half filling at any ϕ . A similar expression for the quadrupole moment has been studied in Refs. 55. However we do not use this approach. Instead we study the nested Wilson loop.

When the Wilson loop spectrum $\nu_x(k_y)$ is gapped, one can compute the nested Wilson loop of the Wilson loop eigenstates that have gaps with other states. The eigenvalues of the nested Wilson loop are denoted as $\nu_y^{\nu_x}$ and $\nu_x^{\nu_y}$. For the selected gapped Wilson loop eigenstates, the sum of the nested Wilson loop eigenvalues determines its quadrupole moment [20]

$$Q_{xy} = \sum_{i=1}^{n_{occ}^{\nu_x}} \nu_y^{\nu_x} = \sum_{i=1}^{n_{occ}^{\nu_y}} \nu_x^{\nu_y} \quad (\text{K3})$$

We choose q -by-1 unit cell for flux $\phi = \frac{2\pi p}{q}$ to compute the Wilson loop spectrum. In Fig. 7 we show the Wilson loop spectrum of the $2q$ valence bands below half filling of the energy spectrum.

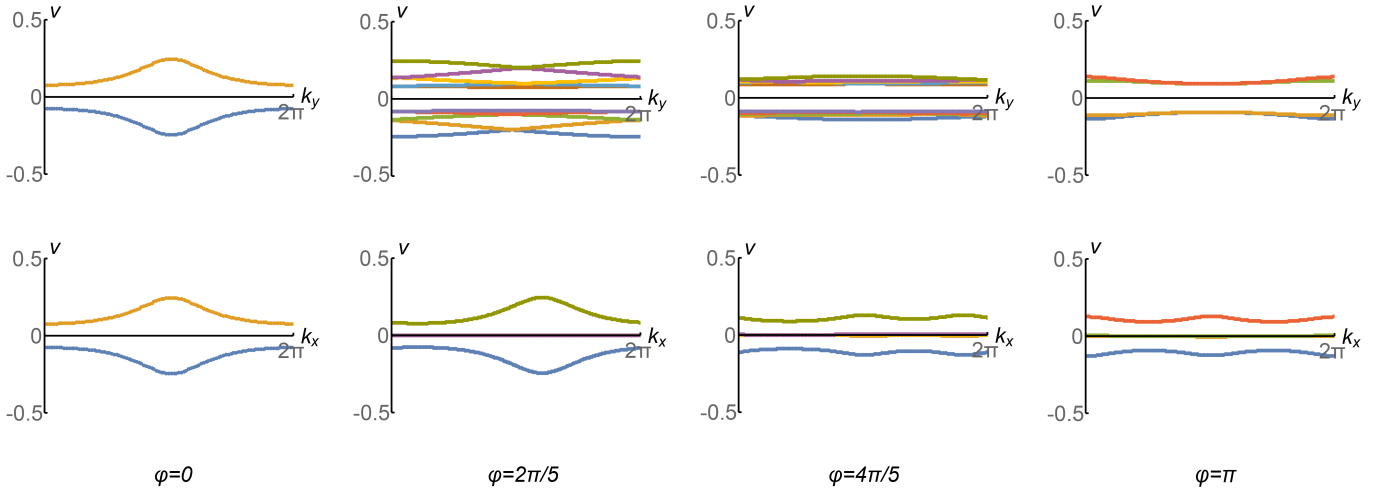


FIG. 7. Wilson loop spectrum for the valence bands at half-filling, directed in x -direction and in y -direction, as defined in Eq. (K1). The upper row corresponds to the spectrum of $W_x(k_y)$, while the lower two row corresponds to the spectrum of $W_y(k_x)$. The critical flux is between $2\pi/5$ and $4\pi/5$.

The Wilson loop spectrum $\nu_x(k_y)$ has a gap at half filling. Therefore, we study the nested Wilson loop $\nu_y^{\nu_x}$ for the q states below this gap. We find that the quadrupole moment Eq. (K3) for the chosen bands is 0.5 when $0 \leq \phi < \phi^*$, and 0 when $\phi^* < \phi < \pi$, where ϕ^* is the critical flux where the Hofstadter spectrum shows the bulk gap closing at half filling.

We now turn to the Wilson loop spectrum $\nu_y(k_x)$ which has two gaps that separate one band on the top, one band on the bottom and $2q - 2$ bands around zero. Therefore, we study the nested Wilson loop $\nu_x^{\nu_y}$ for the single band on the bottom. It turns out that the quadrupole moment Eq. (K3) for the chosen bands is again 0.5 when $0 \leq \phi < \phi^*$, and 0 when $\phi^* < \phi < \pi$.

Appendix L: Magnetic Wannier functions and Balian-Low theorem

In this appendix, we explain the Balian-Low obstruction of exponentially localized Wannier functions in two dimensional systems in a magnetic field. The key ingredient of this theorem is the projective translation group, which bridges our two dimensional magnetic systems and the quantum phase space of one dimensional quantum mechanics where the theorem was originally introduced.

Two-dimensional system under uniform magnetic field have magnetic translation operators that are projective representations of the translation group. The operators satisfy the following multiplication rule

$$T(\mathbf{a}_1)T(\mathbf{a}_2) = T(\mathbf{a}_1 + \mathbf{a}_2)e^{\frac{i}{2}\mathbf{B} \cdot (\mathbf{a}_1 \times \mathbf{a}_2)} \quad (\text{L1})$$

The magnetic unit cell encloses an integer multiple of 2π flux, which ensures that lattice translations commute. Then the momentum space and Bloch wavefunctions are defined. The Bloch wavefunctions in momentum space

Fourier transform into the magnetic Wannier functions in real space.

The quantum phase space of one dimensional quantum mechanics is labeled by two dependent variables, position x and wave vector $k = p/\hbar = -i\frac{d}{dx}$. Now consider the translation operators in the quantum phase space, $T_x(\Delta_x) = e^{-ik\Delta_x}$, $T_k(\Delta_k) = e^{ix\Delta_k}$. The two translations satisfy commutation relation $T_x(\Delta_x)T_k(\Delta_k) = T_k(\Delta_k)T_x(\Delta_x)e^{i\Delta_x\Delta_k}$. More generally, treating x and k on the same footing as $\mathbf{a} = (x_1, x_2) \equiv (x, k)$, the general translations in quantum phase space satisfy the same algebra as given by Eq. (L1)

$$T(\mathbf{a}_1)T(\mathbf{a}_2) = T(\mathbf{a}_1 + \mathbf{a}_2)e^{\frac{i}{2}\mathbf{a}_1 \times \mathbf{a}_2} \quad (\text{L2})$$

where $\mathbf{a}_1 \times \mathbf{a}_2 = -\mathbf{a}_2 \times \mathbf{a}_1$ is a scalar in two dimensions. In one-dimensional quantum mechanics, it was desired to find a set of orthonormal basis functions that are localized in both x and k directions and form a lattice in quantum phase space. The functions are related by discrete translation symmetries

$$g_{m,n}(x) = e^{ixm\Delta_k}g(x - n\Delta_x) \quad (\text{L3})$$

where $g(x)$ is centered at $(0,0)$ and $\Delta_x\Delta_k$ is the size of the unit cell. It was found that the basis is complete if and only if $\Delta_x\Delta_k = 2\pi$ [43]. Lattices satisfying this condition are called von Neumann lattices and the basis functions are also called ‘‘Wannier functions.’’ In the language of time-frequency signal analysis, this set of basis functions $\{g_{m,n}|m,n \in \mathbb{Z}\}$ is also called a Gabor system.

In the quantum phase space (or time-frequency analysis), there is a Balian-Low theorem [44] stating that when $\Delta_x\Delta_k = 2\pi$ for the complete and orthonormal basis of

Hilbert space $\{g_{m,n}|m, n \in \mathbb{Z}\}$,

$$\begin{aligned} & \text{either } \int_{-\infty}^{\infty} x^2 |g(x)|^2 dx = \infty \\ & \text{or } \int_{-\infty}^{\infty} k^2 |\tilde{g}(k)|^2 dk = \infty \end{aligned} \quad (\text{L4})$$

as a consequence of the algebra in Eq. (L2) [56]. This theorem forbids the existence of an exponentially localized Gabor system.

Now return to two-dimensional systems in a magnetic field. It is shown that there is also a Balian-Low theorem that forbids the exponentially localized Wannier function for one band purely due to the algebras of the translation group operators [57]. This result is analogous to the one that has been understood in condensed matter physics.

For a two dimensional lattice system in a magnetic field, each single gapped band has a nonzero Chern number as one can see from the Streda formula. At a rational flux $\phi = 2\pi p/q$, the Streda formula says [58]

$$\bar{\rho} = C \frac{\phi}{2\pi} + s \quad (\text{L5})$$

where $s \in \mathbb{Z}$ for non-interacting systems without symmetry breaking [32]. For a single gapped band $\bar{\rho} = 1/q$. Therefore, we have $Cp = 1 \pmod{q}$.

Interestingly, as Thouless showed in Ref. 59, when the Chern number is nonzero, there are no exponentially localized Wannier functions and the divergence of the variance of either the x or y coordinate is in the form of Eq. (L4) by replacing k with y .